(tetranor-PGDM) の量で評価した。尿中 tetranor-PGDM 量は、LC-MS/MS 法（LC: 資生堂、MS/MS: AB Sciex）によって測定した。各週齢における心機能は、小動物用超音波高解像度イメージングシステム(VISUALSONICS)を用いて、麻酔下で非侵襲的に評価した。

（倫理面への配慮）

実験動物を用いる研究については、国立循環器病研究センターの動物実験指針に準拠して実施した。研究計画は動物実験委員会の承認を得ている。また、麻酔使用等により動物愛護上の倫理的配慮を行い、適切な環境のもとで飼育管理を行った。

C. 研究結果

拡張型心筋症モデルハムスターにおいて、心筋症病態の発症前後（4週齢及び16週齢）で比較すると、16週齢で尿中代謝物量が高くなる傾向が見られた。また、16週齢では野生型ハムスターとの比較でも高値を示した。さらに、2種類の心筋症モデルマウスにおいても検討をはじめたところ、例数は少ないものの、野生型マウスと比べ高値を示す症例が認められた。

心臓組織におけるHPGDSの発現を調べたところ、野生型と比べて、心筋症モデルで高い傾向が確認された。

D. 考察

これらのことから、心筋組織の病変においても、HPGDSによるPGD_2産生が亢進している可能性が示唆された。今後、さらに例数を増やして測定を続けるとともに、心筋組織におけるPGD_2産生と病態進行の関連性を明らかにしていく。

拡張型心筋症は、その発症機序が不明であり予後も不良であることから、新たな治療法の確立が求められている。複数の心筋症モデルで、PGD_2産生の亢進が見られたことから、各種心筋症モデル動物にアスピリン、ステロイド薬、HPGDS 阻害薬の投与実験を行うことで、治療法開発の可能性を検証できる。また、治療対象の決定や薬剤効果を評価できるマーカーが必要であるが、尿中の安定代謝物であるtetranor-PGDMがその候補として期待される。

E. 結論

心筋組織においても骨格筋同様に、筋壊死に伴う病態進行と PGD_2 産生の亢進が関連している可能性が示唆された。

F. 研究発表

1．論文発表

1) Decreased surface sialic acid content is a sensitive indicator for muscle damage. ***Muscle &***

Nerve, 47:372-378, 2013

2) Global metabolic analysis of heart tissue in a hamster model for dilated cardiomyopathy. ***J. Mol. Cell Cardiol.***, 59:76-85,2013

２．学会発表

1) 第 86 回日本薬理学会年会（2013 年 3 月 21-23 日、福岡）「拡張型心筋症モデル動物におけるプロスタグランジン D2 尿中代謝物の増加」

2) 第 86 回日本薬理学会年会（2013 年 3 月 21-23 日、福岡）「筋細胞膜の低下したシアール酸含量は筋変性疾患における傷害の高感度マーカーである」

3) 第 9 回日仏国際シンポジウム（2012 年 9 月 7-8 日、東京）「Inhibition of Ca^{2+}-permeable channel TRPV2 provides the beneficial effects on cardiomyopathy」

G. 知的財産権の出願・登録条件

１．特許取得

1) 特許、第 4997441 号 筋傷害の簡便検査方法及び筋傷害検査用キット　取得日 2012 年 05 月 25 日

２．実用新案登録

なし

３．その他

なし

研究成果の刊行に関する一覧表

雑誌

発表者氏名	論文タイトル名	発表誌名	巻号	ページ	出版年
Nakagawa T, Takeuchi A, Kakiuchi R, Lee T, Yagi M, Awano H, Iijima K, Takeshima Y, Urade Y, Matsuo M	A prostaglandin D_2 metabolite is elevated in the urine of Duchenne muscular dystrophy patients and increases further from 8years old.	***Clin. Chim. Acta.***	423	10-14	2013
Maekawa K, Hirayama A, Iwata Y, Tajima Y, Nishimaki-Mogami T, Sugawara S, Ueno N, Abe H, Ishikawa M, Murayama M, Matsuzawa Y, Nakanishi H, Ikeda K, Arita M, Taguchi R, Minamnimo N, Wakabayashi S, Soga T, Saito Y	Global metabolic analysis of heart tissue in a hamster model for dilated cardiomyopathy.	***J. Mol. Cell Cardiol.***	59	76-85	2013
Iwata Y, Suzuki O, Wakabayashi S	Decreased surface sialic acid content is a sensitive indicator for muscle damage.	***Muscle & Nerve***	47	372-378	2013

Clinica Chimica Acta 423 (2013) 10–14

Contents lists available at SciVerse ScienceDirect

Clinica Chimica Acta

journal homepage: www.elsevier.com/locate/clinchim

A prostaglandin D_2 metabolite is elevated in the urine of Duchenne muscular dystrophy patients and increases further from 8 years old

Taku Nakagawa [a], Atsuko Takeuchi [b], Ryohei Kakiuchi [b], Tomoko Lee [a], Mariko Yagi [a], Hiroyuki Awano [a], Kazumoto Iijima [a], Yasuhiro Takeshima [a], Yoshihiro Urade [c], Masafumi Matsuo [d,*]

[a] Department of Pediatrics, Graduate School of Medicine, Kobe University, Chuo, Kobe 6500017, Japan
[b] Kobe Pharmaceutical University, Higashinada, Kobe 6588558, Japan
[c] Department of Molecular Behavioral Biology, Osaka Bioscience Institute, Suita, Osaka 5650874, Japan
[d] Department of Medical Rehabilitation, Faculty of Rehabilitation, Kobegakuin University, Nishi, Kobe 6512180, Japan

ARTICLE INFO

Article history:
Received 25 January 2013
Received in revised form 27 March 2013
Accepted 27 March 2013
Available online 19 April 2013

Keywords:
Tetranor PGDM
Muscle wasting
Inflammation

ABSTRACT

Background: Duchenne muscular dystrophy (DMD) is a progressive muscle wasting disease caused by muscle dystrophin deficiency. Downstream of the primary dystrophin deficiency is not well elucidated. Here, the hypothesis that prostaglandin D_2 (PGD_2)-mediated inflammation is involved in the pathology of DMD was examined by measuring tetranor PGDM, a major PGD_2 metabolite, in urine of DMD patients.
Methods: We measured tetranor PGDM in urine using LC–MS/MS. First morning urine samples were collected from genetically confirmed DMD patients and age-matched healthy controls aged 4 to 15 y.
Results: The urinary tetranor PGDM concentration was 3.08 ± 0.15 and 6.90 ± 0.35 ng/mg creatinine (mean ± SE) in 79 control and 191 DMD samples, respectively. The mean concentration was approximately 2.2-times higher in DMD patients than in controls ($p < 0.05$). Remarkably, urinary tetranor PGDM concentrations in DMD patients showed chronological changes: it stayed nearly 1.5 times higher than in controls until 7 y but surged at the age of 8 y to a significantly higher concentration.
Conclusion: Urinary tetranor PGDM concentrations were shown to be increased in DMD patients and became higher with advancing age. It was indicated that PGD_2-mediated inflammation plays a role in the pathology of DMD.

1. Introduction

Duchenne muscular dystrophy (DMD; OMIM #310200) is the most common inherited muscle disease, affecting one in every 3500 male births and shows progressive muscle wasting resulting in early death. DMD is characterized by muscle dystrophin deficiency caused by mutations in the *dystrophin* gene, which is the largest human gene consisting of 79 exons. DMD patients all carry disastrous mutations in the *dystrophin* gene, such as frameshift or nonsense mutations [1,2]. However, there is some clinical heterogeneity among DMD patients [3,4] and intrafamilial differences have been observed in patients with an identical dystrophin mutation [5]. Dystrophin is a critical member of the dystrophin glycoprotein complex that creates a direct link between the intracellular cytoskeleton and the extracellular matrix of skeletal muscle. The loss of this connection leaves the muscle fibers susceptible to damage resulting in continuous rounds of muscle degeneration/regeneration.

DMD has been classically considered stereotyped in its clinical presentation, evolution, and severity [6–8]. In a minimal disability stage children are without symptoms or with minimal weakness. In the moderate disability stage, patients are impaired in running and climbing stairs. In the severe disability stage, patients are still ambulant but become increasingly handicapped in their physical activities. In the non-ambulant stage that starts before age 12 y, the children are bed-ridden or wheelchair-bound. This progression process has not been totally explained by a primary loss of dystrophin. Inflammatory and immune responses initiated by aberrant signaling in dystrophic muscle have been considered contributors to disease pathogenesis [9].

Prostaglandin (PG) D_2 (PGD_2) has been implicated in both the development and resolution of inflammation. PGD_2 is synthesized by PGD synthase (PGDS) from PGH_2 that is produced from arachidonic acid by the action of cyclooxygenase and 2 PGDS have been disclosed; lipocalin-type PGDS and hematopoietic PGDS (HPGDS)[10,11]. HPGDS in skeletal muscles was found immunohistochemically stained in some of DMD patients but not in controls [12]. This indicated that the inflammatory mediator PGD_2 plays a role in DMD pathology. However, detailed time-course studies of PGD_2 metabolism in DMD patients are incomplete. Recently, urinary 11,15-dioxo-9α-hydroxy-,2,3,4,5-

* Corresponding author at: Department of Medical Rehabilitation, Faculty of Rehabilitation, Kobegakuin University, 518 Arise, Ikawadani, Nishi, Kobe 651-2180, Japan. Tel./fax: +81 78 974 6194.
E-mail address: mmatsuo@reha.kobegakuin.ac.jp (M. Matsuo).

0009-8981/$ – see front matter © 2013 Elsevier B.V. All rights reserved.
http://dx.doi.org/10.1016/j.cca.2013.03.031

tetranorprostan-1,20-dioic acid (tetranor PGDM) was shown to be a major urinary metabolite of PGD_2 and to reflect its biosynthesis [13].

2. Materials and methods

2.1. Patients

More than 400 DMD patients were referred to the DMD specialist clinic at Kobe University Hospital (Kobe, Japan). Patients were regularly checked for their clinical findings. The causative mutation in the *dystrophin* gene was identified in each case [1]. When corticosteroid use was indicated, predonine was prescribed at 0.5 mg/kg on alternate days. However, fewer than one fifth of patients received corticosteroid therapy in our clinic. One hundred seventeen DMD patients from 4 to 15 y were enrolled in this study and their first morning urines were obtained at 191 points. Age matched 71 male controls were recruited from healthy relatives or volunteers and first morning urine were obtained at 79 points. Two samplings from 1 patient were done at least 6 months separated. Information concerning the clinical condition of the patients and controls was obtained from their parents and hospital records, respectively. Voluntary urine samples or first morning urine samples were collected. Urine samples were stored at −20 °C until analysis. The protocols used in this study were approved by the ethics committee of Kobe University School of Medicine. All urine analysis was conducted after obtaining informed consent from the patients' parents.

2.2. Measurement of urinary tetranor PGDM concentration using mass spectrometry

The urine samples (0.4 ml) diluted with 0.5 ml of water were acidified by the addition of 1 mol/l HCl (final pH ~ 3) and 50 μl (5 ng) of d6-tetranor PGDM and 9,15-dioxo-11α-hydroxy-,2,3,4,5-tetranorprostan-1,20-dioic acid (tetranor PGEM) (Cayman Chemical, Ann Arbor, MI) was added as an internal standard. The mixtures were purified by solid-phase extraction using Sep-Pak Vac 3 cc cartridges (Waters Corp., Milford, MA). The cartridges were pre-conditioned with 3 ml of ethanol and equilibrated with 3 ml of water. The urine sample was applied to the cartridge, which was washed with 6 ml of 5% (v/v) acetonitrile in and then with 6 ml of n-hexane. The analyte and internal standard were eluted from the cartridge with 3 ml of ethyl acetate. The eluate was collected and dried under vacuum. The resulting residue was reconstituted in 100 μl of 10% (v/v) acetonitrile. The sample solution (20 μl) containing tetranor PGDM and tetranor PGEM was then introduced into an API3000 LC–MS/MS system (Applied Biosystems, Foster City, CA) equipped with an electrospray (Turbospray) interface. The HPLC column was a 150 × 2.1-mm i.d. Inertsil ODS-3 (GL Sciences, Tokyo, Japan). LC separation was carried out using a mobile phase consisting of 0.01% (v/v) acetic acid (solvent A) and acetonitrile (solvent B). The following gradient was employed at a flow rate of 250 μl/min: initial (2 min) at 10:95 (A:B); 24 min at 30:70, 27 min at 70:30. The LC–MS/MS was operated in the negative ion mode. The urinary tetranor PGDM was measured in the selected reaction monitoring mode. The transitions monitored were *m/z* 327–143 for the endogenous material and *m/z* 333–149 for the internal standard. The scan time was 250 ms.

The self-prepared samples were used to document the specificity of this method. The linearity of standard calibration curve was examined by analysis of seven concentrations (0.125, 0.250, 0.625, 1.25, 2.50, 6.25 and 12.5 ng/ml). The limit of quantitation defined as the lowest concentration on the calibration curve could be determined with 75–125% of accuracy and CVs < 20%, and the limit of detection was determined at a S/N of 3. The recovery was obtained by experiments using spiked blank matrix with mutually independent replicates at three concentrations of tPGDM (2.50, 6.25 and 12.5 ng/ml). Ten measurements were performed at each of the above 3 concentrations. The intra-day CV of this method was examined using 10 parallel samples at 3 concentrations (2.50, 6.25 and 12.5 ng/ml) prepared as described above. All samples were analyzed on the same day together with the daily calibration; the accuracy and precision were determined at each concentration. Acceptance criteria defined as precision should not exceed 15%, while accuracy should be within 100 ± 15% at each concentration. Acetonitrile (HPLC grade), ethanol, n-hexane, ethyl acetate, and all other chemicals were from Wako Pure Chemical Industries Ltd. (Osaka, Japan).

2.3. Creatinine measurements

Urinary creatinine concentration was measured using a creatinine measurement kit (Wako Pure Chemical Industries Ltd.).

2.4. Statistical analysis

Group difference between DMD patients and healthy children was analyzed using *t*-tests or 2-way analysis of variance in GraphPad Prism 5 (GraphPad Software, Inc., La Jolla, CA). Statistical significance was set at $p < 0.05$.

3. Results

Tetranor PGDM in urine samples was determined in a selected ion monitoring mode by LC–MS/MS. The monitored product ion peaks of tetranor PGDM and tetranor PGEM were clearly separated in the mass chromatogram with each single peak but no interference peaks. The retention time of these peaks of urine samples matched with that of controls (Fig. 1). The concentration of tetranor PGDM was quantitated

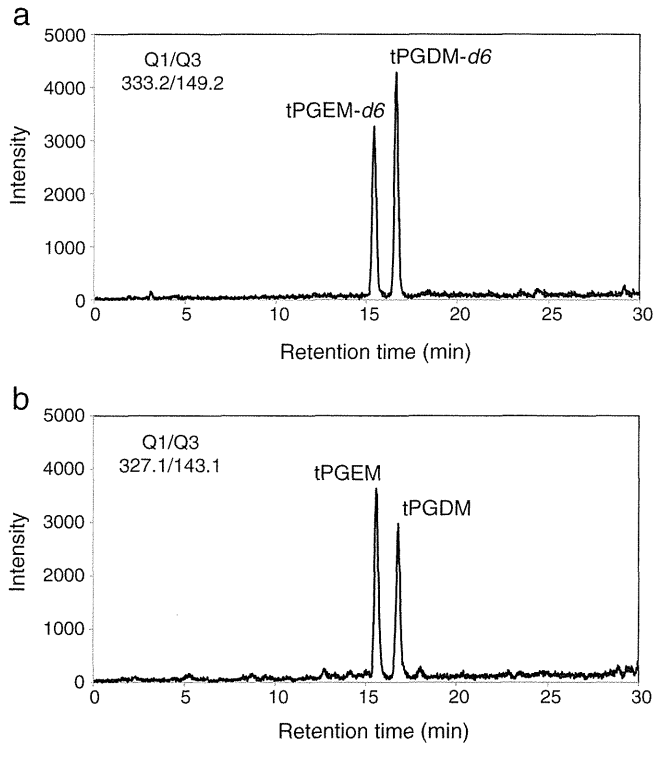

Fig. 1. LC–MS/MS chromatograms. Representative chromatograms of d6-teteranor PGDM and d6-tetranor PGEM (a) and endogenous compounds in urine (b). The first-order MS (Q1) analysis was conducted using negative ion scanning mode to ascertain that the precursor ion peak of d6-tetranor PGDM and tetranor PGDM was $[M-H]^-$ and M-1 of these compounds was 332.2 and 327.1, respectively. The second-order MS (Q2) analysis was done after the collision of precursor ion of the respective PGDM with $[M-H]^-$. Through adjustment of cone voltage and impact energy, the second-order mass chromatogram was obtained, and is shown. The ion transitions (Q1/Q3) of *m/z* 332.2/149.2 and 327.1/143.1 were used to analyze quantitatively and qualitatively, respectively.

using the peak area ratios of tetranor PGDM to d6-tetranor PGDM, on the basis of the calibration curve. The calibration curve was linear in the concentration range of 0.125–12.5 ng/ml (1/x weighting, $y = 0.072x + 0.00503$, $r = 0.997$). The lower limit of quantification reached 0.125 ng/ml. The intra- and the inter-day precision were less than 5.5% and 8.5%, respectively. The current LC–MS/MS method was validated as simple, sensitive, and accurate.

Urinary tetranor PGDM concentrations of DMD patients were determined in samples obtained at voluntary urination. The concentration fluctuated during the day but the first morning urine showed the lowest daytime concentration in all the examined paired samples (data not shown). Therefore, we used the first morning urine for further analyses, as has been suggested for adults [14]. Urine samples were obtained at 191 points from 117 DMD patients aged from 4 to 15 y and 79 points from 71 age-matched healthy children (Fig. 2a). In controls, the concentration of tetranor PGDM was 3.08 ± 0.15 ng/mg creatinine (mean ± SE), with a range of 1.23 to 7.08 ng/mg creatinine. In contrast, the concentration in DMD patients was 6.90 ± 0.35 ng/mg creatinine (range, 0.38 to 26.46 ng/mg creatinine). The mean concentration of tetranor PGDM in DMD patients was approximately 2.2-times higher than that in controls ($p < 0.0001$).

Corticosteroids are administered to DMD patients even though the mechanism of action is unknown [15]. One report suggested that the anti-inflammatory effect of corticosteroids is due to the suppression of prostaglandin-related inflammation [16]. Therefore, we examined whether corticosteroid administration affected the urinary excretion of tetranor PGDM. The average urinary excretion of tetranor PGDM was 5.44 ± 0.81 ($n = 28$) and 7.15 ± 0.38 ($n = 163$) ng/mg creatinine in DMD patients with and without corticosteroid therapy, respectively (Fig. 2b). No significant difference ($p = 0.078$) was found. This indicates that the benefit of our corticosteroid treatment is not observed.

To examine chronological changes, we plotted urinary tetranor PGDM concentrations against the age of the patients (Fig. 3a). The concentration in controls did not change greatly by age. In DMD patients, the tetranor PGDM concentrations were higher at younger ages (4–7 y) than in controls. Remarkably, they surged still higher from age 8 to 9 y, the beginning of the non-ambulant stage, and stayed in high concentration thereafter. Urinary tetranor PGDM was significantly higher in the older age DMD group (age 8–15 y) than in the younger age group (age 4–7 y) (Fig. 3b). In contrast, urinary tetranor PGDM was significantly lower in the older age control group (age 8–15 y) than in the younger age group (age 4–7 y) (Fig. 3b). Our results indicated high production of PGD_2 in DMD patients and suggested a role of PGD_2 in DMD pathology, especially the older DMD patients.

4. Discussion

We established a way to quantitate urinary PGDM using LC–MS/MS without a treatment of urine sample with methoxyamine (Fig. 1). Our quantitation way became suitable for clinical application by avoiding a time- and cost-consuming methoxyamine modification that has been employed [13]. It was found that urinary concentrations of tetranor PGDM were approximately 2.2-times higher in DMD patients than in controls (Fig. 2). Furthermore, it was first shown that urinary tetranor PGDM concentrations in DMD patients chronologically fluctuated (Fig. 2). It was remarkable that concentrations of urinary tetranor PGD_2 increased still further from the age of 8 y. Since the concentration of urinary tetranor PGDM has been reported to reflect the amount of PGD_2 in the body and ultimately reflect the activity of HPGDS [13], our findings indicated high HPGDS activity in the body of DMD patients. Immunohistochemical examination of HPGDS in biopsied skeletal muscle disclosed HPGDS-positive necrotic muscle fibers from DMD patients and myositis patients [12]. However, HPGDS was not stained in skeletal muscles of the control and Fukuyama-type muscular dystrophy [12]. Urinary excretion concentration of tetranor PGDM in DMD patients (Fig. 2) implied a 2.2-times increase in HPGDS. Our findings were also consistent with those of a murine study, in which the urinary concentration of tetranor PGDM was approximately 3-times higher in *mdx* mice than in wild-type mice [16]. This indicates that similar pathogenic mechanisms caused by primary dystrophin deficiency occur in both human and mouse. PGD_2 is considered an important molecule in the pathology of DMD.

Urinary tetranor PGDM has been shown to be increased in adults with inflammatory conditions such as chronic obstructive pulmonary disease, asthma, and amyotrophic lateral sclerosis, and PGD_2 is considered a mediator of inflammation in these conditions [13,14,17,18]. Therefore, increased urinary concentrations of tetranor PGDM in DMD suggested that PGD_2-mediated inflammation plays a role in the pathology of DMD. This finding may pave the way towards understanding the pathogenesis of DMD. However, it was questioned why urinary tetranor PGDM concentration increased by aging. As HPGDS is expressed in necrotic muscle fibers [12], increased urinary PGDM is supposed to relate with abundance of necrotic muscle fibers.

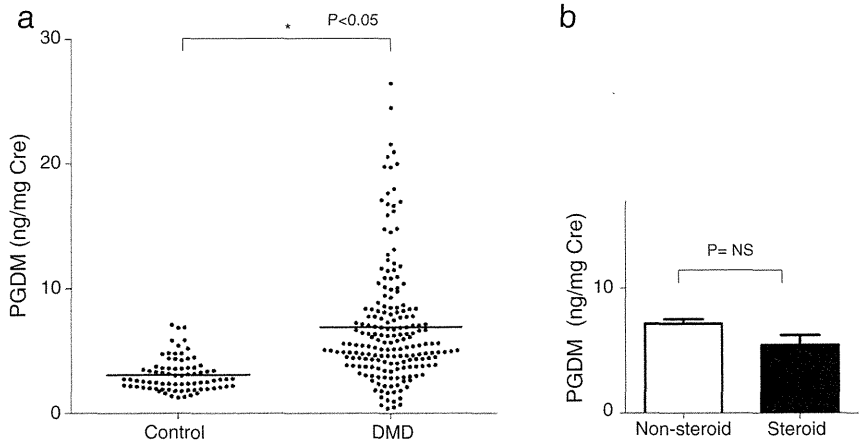

Fig. 2. Urinary tetranor PGDM in DMD patients and healthy children. a. Urinary tetranor PGDM concentration in DMD patients and healthy control children. Individual data points showing urinary tetranor PGDM concentration are represented by circles. In controls, the levels of tetranor PGDM were 3.08 ± 0.15 ng/mg creatinine (mean ± SE) (range, 1.23 to 7.08 ng/mg creatinine), while those were 6.90 ± 0.35 ng/mg creatinine (range, 0.38 to 26.46 ng/mg creatinine) in DMD patients. The mean concentration of tetranor PGDM in DMD patients was approximately 2.2-times higher than that in controls ($p < 0.0001$). The horizontal bars represent the mean. b. Effect of corticosteroid treatment on urinary tetranor PGDM concentration in DMD patients. The average urinary excretion of tetranor PGDM was 5.44 ± 0.81($n = 28$) and 7.15 ± 0.38 ($n = 163$) ng/mg creatinine in DMD patients with (Steroid) and without corticosteroid therapy (Non-steroid), respectively. The data are shown as mean + SE. Bars and horizontal lines represent mean and SE, respectively. There was no significant difference between patients receiving corticosteroid (Steroid) ($n = 28$) or not receiving (Non-steroid) ($n = 163$) corticosteroid treatment.

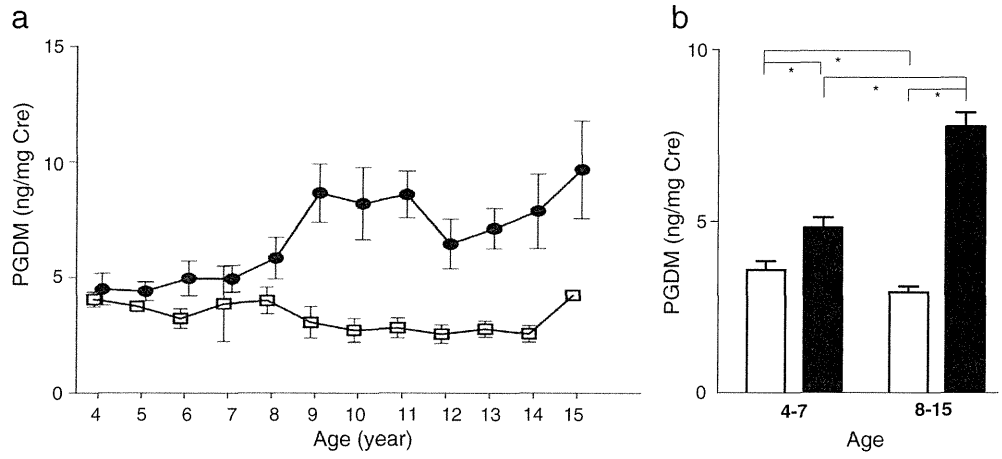

Fig. 3. Chronological changes of urinary tetranor PGDM. a. Chronological changes of mean levels of urinary tetranor PGDM. Mean levels of urinary tetranor PGDM are shown by age in 191 DMD samples (black circles) and 79 control samples (open boxes). The tetranor PGDM levels in DMD patients were higher than controls. Remarkably, they surged still higher from ages 8 to 9, the beginning of the non-ambulant stage, and stayed high level thereafter. However, the tetranor PGDM levels in controls were similar levels throughout the examination period. The data are shown as mean ± SE. b. Comparison of urinary tetranor PGDM concentrations in aged 4 to 7 and 8 to 15 groups. Mean concentration of urinary PGDM in aged 4–7 and 8–15 groups of DMD patients (black columns) and controls (open columns) are shown. In DMD urinary tetranor PGDM was significantly higher in the older age group (age 8–15) ($n = 140$) than in the younger age group (age 4–7) ($n = 51$) (7.69 ± 0.44 vs. 4.75 ± 0.32 ng/mg creatinine (mean ± SE) ($p < 0.05$)). In control, however, urinary tetranor PGDM was significantly lower in the older age group (age 8–15) ($n = 57$) than in the younger age group (age 4–7) ($n = 22$) (2.90 ± 0.17 vs. 3.55 ± 0.30 ng/mg creatinine (mean ± SE) ($p < 0.05$)). The data are represented as mean + SE. Asterisks mean significant difference ($p < 0.05$).

It has been demonstrated that creatinine excretion progressively decreases in parallel with muscle wasting in patients with Duchenne muscular dystrophy [19]. The apparent increase of tetranor PGDM (expressed as ng/mg creatinine) in the DMD patients (Fig. 2) was attributable, at least in part, to the decreased concentrations of creatinine excretion in these patients. Considering that urinary creatinine excretion could be a reliable index of muscle mass [20], urinary tetranor PGDM concentration expressed as ng/mg creatinine was considered to reflect a PGD_2 production in a certain amount of muscle mass. Namely, DMD patients are supposed to have higher HPGDS activity than controls in a certain volume of muscle. Ideally, tetranor PGDM concentrations would have been studied in 24 h urine samples, allowing them also to be expressed as total output per day and hence independent of creatinine concentration. However, it was not considered reasonable to perform 24 h urine collections in this patient population.

HPGDS is widely distributed in various human organs [21]. However, the remarkable increases in HPGDS in DMD boys are observed only in the skeletal muscle [12]. The other type of PGDS, lipocalin-type PGDS, is distributed in the heart, male genital organs, and the central nervous system [22]. Lipocalin-type PGDS is not increased in the DMD muscle. In *mdx* mice, a murine model of DMD, the urinary tetranor PGDM concentration was decreased by administration of an HPGDS inhibitor, HQL-79 [16]. These indicated that urinary tetranor PGDM in DMD is mainly produced by HPGDS-derived PGD_2.

Administration of corticosteroids has been reported to give some benefit to DMD patients [23,24]. The mechanism through which corticosteroids exert their action is still unclear [15]. It has been proposed that corticosteroids alleviate the dystrophy process through immunosuppression and reduction of inflammation [25] or that corticosteroids act directly on muscle fibers by stabilizing sarcolemma [26]. It was reported that corticosteroids suppress the biosynthesis of prostaglandins by suppression of their biosynthesis enzymes including phospholipase A_2 and cyclooxygenase [27]. Therefore, corticosteroids were supposed to decrease urinary tetranor PGDM excretion by suppression of prostaglandin synthesis. However, we found no significant difference in urinary tetranor PGDM concentrations between DMD patients with and without corticosteroid treatment (Fig. 2). This suggested that the benefits of corticosteroid administration are not mediated through PGD_2-related inflammation or that our treatment protocol (0.5 mg/kg on alternative days) is not enough to modulate PGDS. It needs further study to clarify this.

DMD is caused by a deficiency of dystrophin in skeletal muscle. The clinical time-course of DMD is well known [9], but the detailed pathogenesis of the progressive muscle wasting has not been elucidated. Muscle degeneration can be observed before birth [6], but the minimal disability stage occurs between ages 4 and 5 y. Mechanical injury to dystrophin deficient membranes is an important factor promoting dystrophic disease pathology but it does not fully explain DMD disease onset and progression. Aberrant intracellular signaling cascades, which regulate both inflammatory and immune processes, have been considered to contribute substantially to the degenerative process. Observations of upregulated inflammatory genes and activated immune cell infiltrates during critical disease stages in dystrophic muscle suggest that these inflammatory processes may play a critical role in initiating and exacerbating muscle wasting [28–32]. A major limitation in understanding the role of the inflammatory immune response in DMD is the absence of detailed time-course studies before, during, and after the onset of lesion development in the muscles of affected humans. It was remarkable that urinary tetranor PGDM concentrations changed chronologically, with a notable increase from the age of 8 y (Fig. 3a). Our findings are compatible with those of Okinaga et al. who showed HPGDS-positive hyalinated necrotic muscle fibers in all aged DMD patients but not in all younger patients [12]. Taken this into consideration, it was suggested that hyalinated fibers expressing HPGDS increase in skeletal muscles of aged DMD patients.

It has been suggested that cycles of degeneration and regeneration in dystrophic muscle eventually deplete satellite replacement cells (i.e., muscle stem cells) [8,33] and that, once the satellite cells are depleted, muscle regeneration ceases, promoting the progressive replacement of muscle tissue with adipose and fibrous connective tissues [34]. However, the mechanisms regulating the degeneration and regeneration cycles have not been clearly defined [9]. Ages 8 to 9 y when urinary tetranor PGDM surged corresponds to the time when the clinical disability changes from the minimal to the severe disability stage. It was supposed that the surge in production of PGD_2 may relate to this progression. The loss of ambulation was reported to manifest at a mean age of 10.3 y in a recent study on genetically confirmed DMD cases [2]. High plateau concentration of urinary tetranor PGDM corresponded to this non-ambulant stage. Our results suggest that PGD_2-mediated inflammation augments pathophysiology in the advanced stages of DMD. Therefore, chronological changes of urinary tetranor PGDM were considered to reflect clinical progression.

Inhibition of PGD_2 production has been proposed as a target of DMD treatment based on an animal study [16]. Administration of the HPGDS inhibitor HQL-79 was shown to decrease urinary tetranor PGDM concentrations and ameliorate muscle necrosis in *mdx* mice, DMD model mice [16]. Our results showing high production of PGD_2 in DMD provide a rationale for the administration of an HPGDS inhibitor to DMD patients. Recently, a cyclooxygenase inhibitor was shown to be effective in slowing the progression of muscular dystrophy in α-sarcoglycan-null mice [35]. Considering that PGD_2 is synthesized from PGH_2, a product of arachidonic acid generated by cyclooxygenase, inhibition of cyclooxygenase is another choice for the suppression of PGH_2, leading to a decrease in PGD_2. Aspirin has been shown to decrease urinary tetranor PGDM concentrations significantly [16], and to ameliorate muscle morphology in *mdx* mice [36]. So this common drug may also be useful for the treatment of DMD.

5. Conclusion

Urinary tetranor PGDM concentrations were increased in DMD patients and became higher with advancing age. It was indicated that PGD_2-mediated inflammation plays a role in the pathology of DMD. It was supposed that hyalinated fibers expressing HPGDS increase in older DMD patients.

List of abbreviations

DMD Duchenne muscular dystrophy
PG prostaglandin
HPGDS hematopoietic prostaglandin D synthase
tetranor PGDM 11,15-dioxo-9α-hydroxy-,2,3,4,5-tetranorprostan-1,20-dioic acid
tetranor PGEM 9,15-dioxo-11α-hydroxy-,2,3,4,5-tetranorprostan-1,20-dioic acid.

Acknowledgments

We thank all the participating families and the Happy Smile Club. We are grateful to Drs. Shinya Kamauchi and Kousuke Aritake (Department of Molecular Behavioral Biology, Osaka Bioscience Institute, Suita, Osaka, Japan) for their valuable suggestions. This work was supported by a Grant-in-Aid for Scientific Research (B), and a Grant-in-Aid for Exploratory Research from the Japan Society for the Promotion of Science, a Health and Labour Sciences Research Grant for Research on Psychiatric and Neurological Diseases and Mental Health, and a research grant for Nervous and Mental Disorders from the Ministry of Health, Labour, and Welfare, Japan.

References

[1] Takeshima Y, Yagi M, Okizuka Y, et al. Mutation spectrum of the dystrophin gene in 442 Duchenne/Becker muscular dystrophy cases from one Japanese referral center. J Hum Genet 2010;55:379–88.
[2] Magri F, Govoni A, D'Angelo MG, et al. Genotype and phenotype characterization in a large dystrophinopathic cohort with extended follow-up. J Neurol 2011;258:1610–23.
[3] Nishiyama A, Takeshima Y, Zhang Z, et al. Dystrophin nonsense mutations can generate alternative rescue transcripts in lymphocytes. Ann Hum Genet 2008;72:717–24.
[4] Desguerre I, Christov C, Mayer M, et al. Clinical heterogeneity of Duchenne muscular dystrophy (DMD): definition of sub-phenotypes and predictive criteria by long-term follow-up. PLoS One 2009;4:e4347.
[5] Sifringer M, Uhlenberg B, Lammel S, et al. Identification of transcripts from a subtraction library which might be responsible for the mild phenotype in an intrafamilially variable course of Duchenne muscular dystrophy. Hum Genet 2004;114:149–56.
[6] Brooke MH, Fenichel GM, Griggs RC, et al. Clinical investigation in Duchenne dystrophy: 2. Determination of the "power" of therapeutic trials based on the natural history. Muscle Nerve 1983;6:91–103.
[7] Mendell JR, Province MA, Moxley III RT, et al. Clinical investigation of Duchenne muscular dystrophy. A methodology for therapeutic trials based on natural history controls. Arch Neurol 1987;44:808–11.
[8] Bell CD, Conen PE. Histopathological changes in Duchenne muscular dystrophy. J Neurol Sci 1968;7:529–44.
[9] Evans NP, Misyak SA, Robertson JL, Bassaganya-Riera J, Grange RW. Dysregulated intracellular signaling and inflammatory gene expression during initial disease onset in Duchenne muscular dystrophy. Am J Phys Med Rehabil 2009;88:502–22.
[10] Urade Y, Ujihara M, Horiguchi Y, et al. Mast cells contain spleen-type prostaglandin D synthetase. J Biol Chem 1990;265:371–5.
[11] Urade Y, Hayaishi O. Prostaglandin D synthase: structure and function. Vitam Horm 2000;58:89–120.
[12] Okinaga T, Mohri I, Fujimura H, et al. Induction of hematopoietic prostaglandin D synthase in hyalinated necrotic muscle fibers: its implication in grouped necrosis. *Acta Neuropathol* 2002;104:377–84.
[13] Song WL, Wang M, Ricciotti E, et al. Tetranor PGDM, an abundant urinary metabolite reflects biosynthesis of prostaglandin D2 in mice and humans. J Biol Chem 2008;283:1179–88.
[14] Shinozawa T, Urade Y, Maruyama T, Watabe D. Tetranor PGDM analyses for the amyotrophic lateral sclerosis: positive and simple diagnosis and evaluation of drug effect. Biochem Biophys Res Commun 2011;415:539–44.
[15] Moxley III RT, Pandya S, Ciafaloni E, Fox DJ, Campbell K. Change in natural history of Duchenne muscular dystrophy with long-term corticosteroid treatment: implications for management. J Child Neurol 2010;25:1116–29.
[16] Mohri I, Aritake K, Taniguchi H, et al. Inhibition of prostaglandin D synthase suppresses muscular necrosis. Am J Pathol 2009;174:1735–44.
[17] Zhang Y, Zhang G, Clarke PA, et al. Simultaneous and high-throughput quantitation of urinary tetranor PGDM and tetranor PGEM by online SPE-LC–MS/MS as inflammatory biomarkers. J Mass Spectrom 2011;46:705–11.
[18] Higashi N, Mita H, Yamaguchi H, Fukutomi Y, Akiyama K, Taniguchi M. Urinary tetranor-PGDM concentrations in aspirin-intolerant asthma and anaphylaxis. J Allergy Clin Immunol 2012;129:557–9.
[19] Griggs RC, Forbes G, Moxley RT, Herr BE. The assessment of muscle mass in progressive neuromuscular disease. Neurology 1983;33:158–65.
[20] Wang ZM, Gallagher D, Nelson ME, Matthews DE, Heymsfield SB. Total-body skeletal muscle mass: evaluation of 24-h urinary creatinine excretion by computerized axial tomography. Am J Clin Nutr 1996;63:863–9.
[21] Kanaoka Y, Fujimori K, Kikuno R, Sakaguchi Y, Urade Y, Hayaishi O. Structure and chromosomal localization of human and mouse genes for hematopoietic prostaglandin D synthase. Conservation of the ancestral genomic structure of sigma-class glutathione S-transferase. Eur J Biochem 2000;267:3315–22.
[22] Smith WL, Urade Y, Jakobsson PJ. Enzymes of the cyclooxygenase pathways of prostanoid biosynthesis. Chem Rev 2011;111:5821–65.
[23] Manzur AY, Kuntzer T, Pike M, Swan A. Glucocorticoid corticosteroids for Duchenne muscular dystrophy.Cochrane Database Syst Rev 2008(1) [CD003725].
[24] Escolar DM, Hache LP, Clemens PR, et al. Randomized, blinded trial of weekend vs daily prednisone in Duchenne muscular dystrophy. Neurology 2011;77:444–52.
[25] Iannitti T, Capone S, Feder D, Palmieri B. Clinical use of immunosuppressants in Duchenne muscular dystrophy. J Clin Neuromuscul Dis 2010;12:1–21.
[26] Jacobs SC, Bootsma AL, Willems PW, Bar PR, Wokke JH. Prednisone can protect against exercise-induced muscle damage. J Neurol 1996;243:410–6.
[27] Masferrer JL, Seibert K, Zweifel B, Needleman P. Endogenous glucocorticoids regulate an inducible cyclooxygenase enzyme. Proc Natl Acad Sci U S A 1992;89:3917–21.
[28] Spencer MJ, Montecino-Rodriguez E, Dorshkind K, Tidball JG. Helper (CD4(+)) and cytotoxic (CD8(+)) T cells promote the pathology of dystrophin-deficient muscle. Clin Immunol 2001;98:235–43.
[29] Porter JD, Merriam AP, Leahy P, Gong B, Khanna S. Dissection of temporal gene expression signatures of affected and spared muscle groups in dystrophin-deficient (mdx) mice. Hum Mol Genet 2003;12:1813–21.
[30] Chen YW, Nagaraju K, Bakay M, et al. Early onset of inflammation and later involvement of TGFbeta in Duchenne muscular dystrophy. Neurology 2005;65:826–34.
[31] Pescatori M, Broccolini A, Minetti C, et al. Gene expression profiling in the early phases of DMD: a constant molecular signature characterizes DMD muscle from early postnatal life throughout disease progression. FASEB J 2007;21:1210–26.
[32] Lawler JM. Exacerbation of pathology by oxidative stress in respiratory and locomotor muscles with Duchenne muscular dystrophy. J Physiol 2011;589:2161–70.
[33] Webster C, Silberstein L, Hays AP, Blau HM. Fast muscle fibers are preferentially affected in Duchenne muscular dystrophy. Cell 1988;52:503–13.
[34] Collins CA, Morgan JE. Duchenne's muscular dystrophy: animal models used to investigate pathogenesis and develop therapeutic strategies. Int J Exp Pathol 2003;84:165–72.
[35] Sciorati C, Miglietta D, Buono R, et al. A dual acting compound releasing nitric oxide (NO) and ibuprofen, NCX 320, shows significant therapeutic effects in a mouse model of muscular dystrophy. Pharmacol Res 2011;64:210–7.
[36] Serra F, Quarta M, Canato M, et al. Inflammation in muscular dystrophy and the beneficial effects of non-steroidal anti-inflammatory drugs. Muscle Nerve 2012;46:773–84.

Journal of Molecular and Cellular Cardiology 59 (2013) 76–85

Contents lists available at SciVerse ScienceDirect

Journal of Molecular and Cellular Cardiology

journal homepage: www.elsevier.com/locate/yjmcc

Original article

Global metabolomic analysis of heart tissue in a hamster model for dilated cardiomyopathy

Keiko Maekawa [a,1], Akiyoshi Hirayama [b,1], Yuko Iwata [c,1], Yoko Tajima [a], Tomoko Nishimaki-Mogami [a], Shoko Sugawara [b], Noriko Ueno [a], Hiroshi Abe [b], Masaki Ishikawa [a], Mayumi Murayama [a], Yumiko Matsuzawa [a], Hiroki Nakanishi [a,d], Kazutaka Ikeda [b], Makoto Arita [a,e], Ryo Taguchi [a,f], Naoto Minamino [c], Shigeo Wakabayashi [c], Tomoyoshi Soga [b,*,1], Yoshiro Saito [a,**,1]

[a] Project Team for Disease Metabolomics, National Institute of Health Sciences, Tokyo 158-8501, Japan
[b] Institute for Advanced Biosciences, Keio University, Tsuruoka, Yamagata 997-0052, Japan
[c] National Cerebral and Cardiovascular Center Research Institute, Suita, Osaka 565-8565, Japan
[d] Bioscience and Research Center, Akita University, Akita 010-8543, Japan
[e] Department of Health Chemistry, Graduate School of Pharmaceutical Sciences, University of Tokyo, Tokyo 113-0033, Japan
[f] College of Life and Health Sciences, Chubu University, Kasugai, Aichi 487-8501, Japan

ARTICLE INFO

Article history:
Received 19 September 2012
Received in revised form 8 January 2013
Accepted 6 February 2013
Available online 20 February 2013

Keywords:
Dilated cardiomyopathy
Hamster model
Metabolomics
Oxidative stress
Phospholipid alteration

ABSTRACT

Dilated cardiomyopathy (DCM), a common cause of heart failure, is characterized by cardiac dilation and reduced left ventricular ejection fraction, but the underlying mechanisms remain unclear. To investigate the mechanistic basis, we performed global metabolomic analysis of myocardial tissues from the left ventricles of J2N-k cardiomyopathic hamsters. This model exhibits symptoms similar to those of human DCM, owing to the deletion of the δ-sarcoglycan gene. Charged and lipid metabolites were measured by capillary electrophoresis mass spectrometry (MS) and liquid chromatography MS(/MS), respectively, and J2N-k hamsters were compared with J2N-n healthy controls at 4 (presymptomatic phase) and 16 weeks (symptomatic) of age. Disturbances in membrane phospholipid homeostasis were initiated during the presymptomatic phase. Significantly different levels of charged metabolites, occurring mainly in the symptomatic phase, were mapped to primary metabolic pathways. Reduced levels of metabolites in glycolysis, the pentose phosphate pathway, and the tricarboxylic acid cycle, together with large decreases in major triacylglycerol levels, suggested that decreased energy production leads to cardiac contractile dysfunction in the symptomatic phase. A mild reduction in glutathione and a compensatory increase in ophthalmate levels suggest increased oxidative stress in diseased tissues, which was confirmed by histochemical staining. Increased levels of 4 eicosanoids, including prostaglandin (PG) E_2 and 6-keto-$PGF_{1\alpha}$, in the symptomatic phase suggested activation of the protective response pathways. These results provide mechanistic insights into DCM pathogenesis and may help identify new targets for therapeutic intervention and diagnosis.

1. Introduction

Dilated cardiomyopathy (DCM), a common cause of heart failure and a prevalent cardiomyopathy [1], is characterized by left ventricular dilation, impaired cardiac pump function, and a thin cardiac wall, which result in severe contractile dysfunction. β-Blockers constitute a common treatment [2], but severely affected patients may undergo heart transplantation or implantation of left ventricular assist devices. While the underlying etiological factors remain largely unknown, and both familial and non-familial factors are associated with DCM, some proposed disease mechanisms include coronary artery disease, genetic mutation, and viral infection [3]. Mutations in sarcomeric and cytoskeletal genes cause hypertrophic and dilated cardiomyopathies, respectively [4]. Some familial DCM cases are caused by mutations in genes encoding components of the dystrophin–glycoprotein complex (DGC), which spans the sarcolemma linking the extracellular matrix and cytoskeleton and provides mechanical strength for contraction [5]. Mutations in dystrophin, a major cytoskeletal component of the DGC, lead to a high incidence of X-linked DCM in patients with

* Correspondence to: T. Soga, Institute for Advanced Biosciences, Keio University, 246-2 Mizukami, Kakuganji, Tsuruoka, Yamagata 997-0052, Japan. Tel.: +81 235 29 0528; fax: +81 235 29 0574.
** Correspondence to: Y. Saito, Project Team for Disease Metabolomics, National Institute of Health Sciences, 1-18-1 Kamiyoga, Setagaya-ku, Tokyo 158-8501, Japan. Tel.: +81 3 3700 9528; fax: +81 3 3700 9788.
E-mail addresses: soga@sfc.keio.ac.jp (T. Soga), yoshiro@nihs.go.jp (Y. Saito).
[1] Contributed equally to this work.

0022-2828/$ – see front matter © 2013 Elsevier Ltd. All rights reserved.
http://dx.doi.org/10.1016/j.yjmcc.2013.02.008

Duchenne or Becker muscular dystrophy. Mutations in other DGC genes, including *δ-sarcoglycan*, are also associated with human DCM [1].

Oxidative stress is also reported to be involved in DCM pathogenesis. Patients with DCM exhibit increased plasma glutathione levels and lipid peroxidation products such as malondialdehyde [6], and total plasma peroxide levels are inversely correlated with the cardiac ejection fraction [7]. However, a contrasting study found that human left ventricular DCM tissue showed normal glutathione peroxidase and superoxide dismutase activities and malondialdehyde levels similar to those found in healthy control tissue [8]. Thus, the role of oxidative stress in DCM pathogenesis remains to be elucidated.

Animal models with a pathophysiology similar to human DCM are useful for investigating pathogenic mechanisms. A J2N-k DCM hamster and J2N-n control line were established by repeated sib mating of J2N(N8), produced by cross-breeding BIO14.6 cardiomyopathic and normal golden hamsters [9]. J2N-k hamsters are deficient in δ-sarcoglycan and are an animal model of human limb-girdle muscular dystrophy–associated cardiomyopathy. They begin showing heart tissue fibrosis and exhibit moderate cardiac dysfunction at 8–9 weeks of age. At 20 weeks, J2N-k hamsters exhibit considerable fibrosis, a reduced number of cardiomyocytes, and hypertrophic changes in the remaining cardiomyocytes; no such changes occur in J2N-n heart tissues [9]. Accordingly, the life span of J2N-k hamsters (ca. 298 days) is much shorter than that of J2N-n hamsters (ca. 788 days). Besides the *δ-sarcoglycan* gene, J2N-k and J2N-n hamsters have very similar genetic backgrounds. Since mutations in *δ-sarcoglycan* are also detected in DCM patients, J2N-k hamsters are an ideal DCM disease model.

To gain an insight into the DCM in metabolic pathway basis, we performed global metabolomic analysis of myocardial tissues from the left ventricles of J2N-k and J2N-n hamsters. Capillary electrophoresis-time-of-flight mass spectrometry (CE-TOFMS) [10] and liquid chromatography (LC)-TOFMS or triple quadrupole MS/MS were used to measure levels of charged (e.g., amino acids) and lipid (e.g., phospholipids) metabolites, respectively. We identified significant changes in several metabolite levels in age-matched J2N-k and J2N-n hamsters.

2. Methods

2.1. Animals

Male 3- and 15-week-old J2N-k cardiomyopathic hamsters and age-matched J2N-n controls were purchased from Nihon SLC Inc. (Hamamatsu, Japan). All animals were maintained in a specific pathogen-free facility under controlled conditions (20–24 °C and 40–70% humidity) with a 12-h light cycle and were given free access to standard laboratory rat chow (MF, Oriental Yeast, Tokyo, Japan) and tap water. After 1 week of habituation, 4- and 16-week-old animals were anesthetized by intraperitoneal injection of pentobarbital (Dainippon Sumitomo Pharma, Osaka, Japan) at a dose of 50 mg/kg, and the left ventricle was excised. The isolated tissue was processed for either histological analysis (N = 4) or for metabolomic and western blot analysis (N = 7). For metabolomic analysis, tissue was randomly divided into 2 samples and minced on ice to measure charged and lipid metabolites. The tissue samples were weighed and snap frozen in liquid nitrogen before being stored at −80 °C. All animal experiments were performed in accordance with the Guide for the Care and Use of Laboratory Animals published by the US National Institutes of Health (NIH Publication No. 85-23, revised 1996) and the Guidelines for Animal Experimentation and under the control of the Ethics Committee of Animal Care and Experimentation of the National Cerebral and Cardiovascular Center, Japan (Approval number, 12056).

2.2. Echocardiography and histochemical staining

Cardiac function was assessed by echocardiography measurements as shown in the supplementary information. Following this procedure, J2N-k and J2N-n hamsters were sacrificed as described above, and ventricle tissue (from both hamster lines) was processed for Masson's trichrome staining to detect fibrosis, 4-hydroxynonenal (4-HNE) staining to estimate lipid peroxidation [11], and dihydroethidium (DHE) staining to approximate superoxide production [12] as described in the supplementary information.

2.3. Metabolite extraction and quantification

Detailed information regarding the extraction and quantification of charged and lipid metabolites has been provided in the supplementary information. Briefly, charged metabolites were extracted by homogenizing myocardial tissue in methanol and subjected to CE-TOFMS, as previously described [10,13,14]. Lipid metabolite extraction was performed using the Bligh and Dyer method [15] with minor modifications. Lower organic and upper aqueous layers were analyzed by LC-TOFMS and LC-MS/MS for phospholipids/sphingolipids/triacylglycerols and oxidative fatty acids, respectively. Structural analysis of phospholipids (PLs) and sphingomyelins (SMs) was performed as previously described [16].

2.4. Data analysis

Datasets obtained from CE-TOFMS were processed using our proprietary software, MasterHands [17] as shown in the supplementary information. Hydrophilic metabolite concentrations have been provided as the amount of metabolite (μmol) per gram of tissue.

LC-TOFMS data were processed using the 2DICAL software (Mitsui Knowledge Industry, Tokyo, Japan) [18] as described in the supplementary information. Extracted ion peaks were normalized using internal standards (ISs). Metabolites eluting from 0.1 to 37.5 min and from 37.5 to 60 min for LC were normalized to 1, 2-dipalmitoyl-[$^2H_6$]-sn-glycero-3-phosphocholine (16:0-16:0PC-d6; Larodan Fine Chemicals, Malmo, Sweden) and 1,2-caprylin-3-linolein, respectively. Some oxidative fatty acids were quantified using commercially available standards.

2.5. Statistical and multiple classification analyses

Student's *t*-test was used for two-class comparisons between J2N-n and J2N-k at each growth stage (4 and 16 weeks), and $p<0.05$ was deemed as statistically significant. The multiple testing correction was not applied since metabolite levels are not exclusive but rather related with each other, and we focused on revealing overall metabolic changes (such as pathways or metabolite groups) in the cardiomyocytes from J2N-k hamsters compared to J2N-n cardiomyocytes. In addition, data were imported into the SIMCA-P+ software (Version 12.0; Umetrics, Umeå, Sweden), pareto-scaled, and subjected to principal component analysis (PCA; short explanation is provided in the supplementary information). Cluster analysis and heatmap representations were obtained using the Spotfire software (Version 7.1; TIBCO, MA, USA).

3. Results

3.1. Cardiac function and pathophysiology of J2N-n and J2N-k hamsters

In this study, the 4- and 16-weeks of ages were selected as DCM presymptomatic and symptomatic phases for J2N-k (and its control J2N-n) hamsters according to the previous paper [9]. First, we examined cardiac function of both hamsters at these time points. Echocardiograph measurements of J2N-k hamsters at 16 weeks revealed a significant increase in the internal diameter of the left ventricle (LVID) during both diastolic and systolic states; however, this

Table 1
Summary of echocardiographic analysis.

		4 weeks	4 weeks	16 weeks	16 weeks	
		J2N-n	J2N-k	J2N-n	J2N-k	*p* values
LVIDd	mm	3.10 ± 0.05	2.89 ± 0.23	3.80 ± 0.36	5.07 ± 0.26	0.0291*
LVIDs	mm	1.49 ± 0.10	1.21 ± 0.20	2.06 ± 0.18	3.64 ± 0.21	0.0013**
LVPWd	mm	1.85 ± 0.18	1.82 ± 0.31	2.09 ± 0.30	1.77 ± 0.09	0.3487
LVPWs	mm	2.22 ± 0.11	2.08 ± 0.22	2.28 ± 0.27	1.95 ± 0.13	0.3285
EF	%	77.64 ± 1.43	83.68 ± 3.07	77.64 ± 1.44	54.46 ± 1.04	<0.0001***
FS	%	51.80 ± 3.53	58.41 ± 5.63	45.62 ± 1.41	28.35 ± 0.60	<0.0001***
LV VOLd	μL	38.03 ± 1.46	32.81 ± 6.57	64.50 ± 14.69	123.70 ± 15.58	0.0327*
LV VOLs	μL	6.13 ± 1.08	4.01 ± 1.53	14.31 ± 2.94	56.69 ± 8.27	0.0029**

LVIDd, left ventricular internal diameter in diastole; LVIDs, left ventricular internal diameter in systole; LVPWd, left ventricular posterior wall in diastole; LVPWs, left ventricular posterior wall in systole; EF, ejection fraction; FS, fractional shortening (given by (LVIDd-LVIDs)/LVIDd × 100); LV VOLd, left ventricular volume in diastole; LV VOLs, left ventricular volume in systole. *p* values are analyzed between 16 week-old J2N-k and J2N-n hamsters. In 4 week-old hamsters, the *p* values are not significant.
* $p<0.05$.
** $p<0.005$.
*** $p<0.0001$.

was not observed at 4 weeks of age (Table 1). In addition, markedly reduced ejection fractions and fractional shortening were revealed at 16 weeks (Table 1 and Supplementary Fig. 1). Extensive fibrosis was observed in J2N-k hamsters at 16 weeks (compared to the J2N-n) by Masson's trichrome staining (Supplementary Fig. 2). No fibrosis was observed at 4 weeks. Thus, no obvious pathophysiological change was observed at 4 weeks, although DCM was obvious at 16 weeks in J2N-k hamsters.

3.2. Profiling of charged metabolites measured by CE-TOFMS

Charged metabolite levels were quantified absolutely using standard chemicals for each metabolite, whereas lipid metabolite levels were quantified relatively as ratios of ion counts (peak height) of each metabolite to those of the internal standard, with the exception of some oxidative fatty acids. Therefore, statistical analyses of charged and lipid metabolites were carried out separately.

A total of 180 charged metabolites were identified and quantified by the CE-TOFMS method (Supplementary Table 2). Using a whole dataset of quantified metabolites, we performed a PCA (Supplementary Fig. 3) in order to understand the similarities/dissimilarities of 4 animal groups regarding variations in metabolite levels. From the PCA score plot, DCM and control hamsters at 16 weeks (but not at 4 weeks) were separated in the first 2 principal components. This analysis indicates that the profiles of charged metabolites reflect the metabolic differences caused by disease progression.

Next, Student's *t*-test was used to examine DCM-associated metabolic changes (Supplementary Table 2). Using a *p*-value threshold of 0.01 to generate a heatmap (Fig. 1A), the levels of 15 metabolites were found to differ between J2N-k and J2N-n hamsters at 4 weeks; specifically, the level of 12 metabolites increased and 3 metabolites decreased in J2N-k hamsters. At the symptomatic phase (16 weeks), 62 metabolites were detected at different levels ($p<0.01$) in J2N-k and J2N-n hamsters (Fig. 1B), including 10 metabolites that also showed significant differences in the presymptomatic phase (4 weeks; 2-aminobutyrate (2-AB), citrulline, guanidinoacetate, hypotaurine, methionine, *N*-acetylaspartate, ophthalmate, ornithine, threonine, and trigonelline). Of the 62 metabolites showing variation, the levels of 26 increased and 36 decreased in the J2N-k hamsters. Most of these metabolites are components of primary metabolic pathways such as glycolysis, the pentose phosphate pathway, the tricarboxylic acid (TCA) cycle, the glutathione biosynthesis pathway, and the urea cycle.

3.3. Energy metabolism

J2N-k myocardial tissues from 16-week-old animals exhibited changes in the levels of metabolic intermediates involved in energy metabolism. The concentrations of several intermediates involved in glycolysis, such as glucose 6-phopshate (G6P; levels of J2N-k/J2N-n = 0.5-fold, $p=5.9\times10^{-5}$), dihydroxyacetone phosphate (DHAP; 0.6-fold, $p=1.4\times10^{-3}$), and acetyl CoA (0.3-fold, $p=1.1\times10^{-5}$), were significantly reduced at 16 weeks but not at 4 weeks (Fig. 2).

Significantly decreased levels of the TCA cycle intermediates, isocitrate (0.6-fold, $p=1.5\times10^{-6}$) and malate (0.7-fold, $p=2.5\times10^{-3}$), were also observed in myocardial tissues from 16-week-old J2N-k hamsters. Decreased protein levels of aconitase 2, which catalyzes citrate to isocitrate via *cis*-aconitate, were observed at 16 weeks in the J2N-k, suggesting decreased TCA cycle activity (Supplementary Fig. 4). These results suggest that the levels of metabolites involved in glycolysis and the TCA cycle energy pathways are attenuated in J2N-k cardiomyopathic tissue during the symptomatic phase.

3.4. Glutathione biosynthesis pathway

The ophthalmate and 2-AB levels were significantly higher in J2N-k myocardial tissues than in J2N-n control tissue at both the presymptomatic (1.4-fold, $p=2.6\times10^{-3}$; 2.2-fold, $p=6.9\times10^{-5}$, respectively) and symptomatic (2.3-fold, $p=3.9\times10^{-7}$; 4.2-fold, $p=2.2\times10^{-9}$, respectively) phases (Fig. 3). 2-AB is metabolized to ophthalmate via γ-Glu-2-AB through a 2-step reaction and then catalyzed sequentially by γ-glutamylcysteine synthetase and glutathione synthetase [10]. In contrast, γ-Glu-Cys and glutathione (GSH) concentrations are decreased at 16 weeks (0.2-fold, $p=7.9\times10^{-3}$; 0.8-fold, $p=2.0\times10^{-2}$, respectively). These data suggest that upregulation of the GSH biosynthetic pathway is associated with DCM progression. Consistent with this observation, intracellular levels of glycine (1.3-fold, $p=1.2\times10^{-5}$), methionine (1.3-fold, $p=2.9\times10^{-5}$), and *S*-adenosylhomocysteine (SAH; 1.2-fold, $p=2.4\times10^{-2}$) were elevated in J2N-k hamsters at 16 weeks. In contrast, *S*-adenosylmethionine (SAM; 0.9-fold, $p=3.2\times10^{-2}$) levels were reduced at the symptomatic-phase in J2N-k hamsters.

Taurine levels did not differ significantly between the 2 genotypes, although increased concentrations of its precursor, hypotaurine, were observed in J2N-k hamsters at both 4 weeks (1.6-fold, $p=6.9\times10^{-5}$) and 16 weeks (3.4-fold, $p=1.6\times10^{-9}$).

3.5. Urea cycle

The levels of most urea cycle intermediates significantly differed between myocardial tissues from J2N-k and J2N-n at 16 weeks (Fig. 4). The levels of arginine (0.7-fold, $p=3.2\times10^{-5}$), citrulline (0.6-fold, $p=2.0\times10^{-5}$), and argininosuccinate (0.4-fold, $p=6.3\times10^{-4}$) were significantly reduced in J2N-k hamsters. In contrast, ornithine levels (1.8-fold, $p=8.2\times10^{-8}$) were significantly increased. At 4 weeks, a

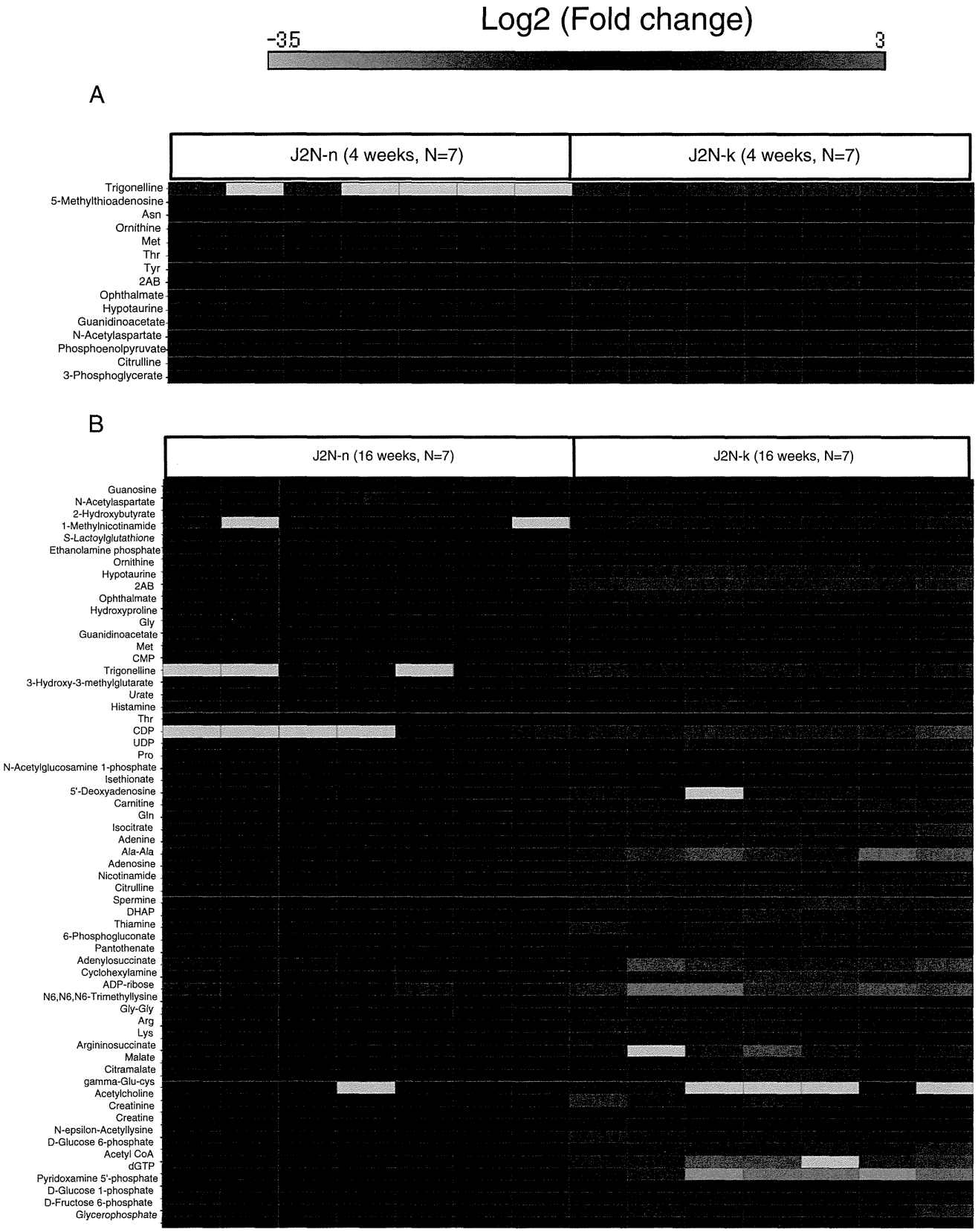

Fig. 1. Heatmap showing charged metabolites in myocardial tissues from J2N-n and J2N-k hamsters at (A) 4 weeks and (B) 16 weeks ($n=7$ in all groups). Fold changes in the amounts of each metabolite in individual J2N-k samples, relative to the average amounts in J2N-n at either 4 or 16 weeks are represented as the log2 ratio. Light gray cells indicate that metabolites were not detected in those samples. Fifteen (at 4 weeks) and sixty-two (at 16 weeks) charged metabolites that showed different levels ($p<0.01$) at each time point are shown, excluding Glu–Glu at 16 weeks, which was not detected in all J2N-n samples.

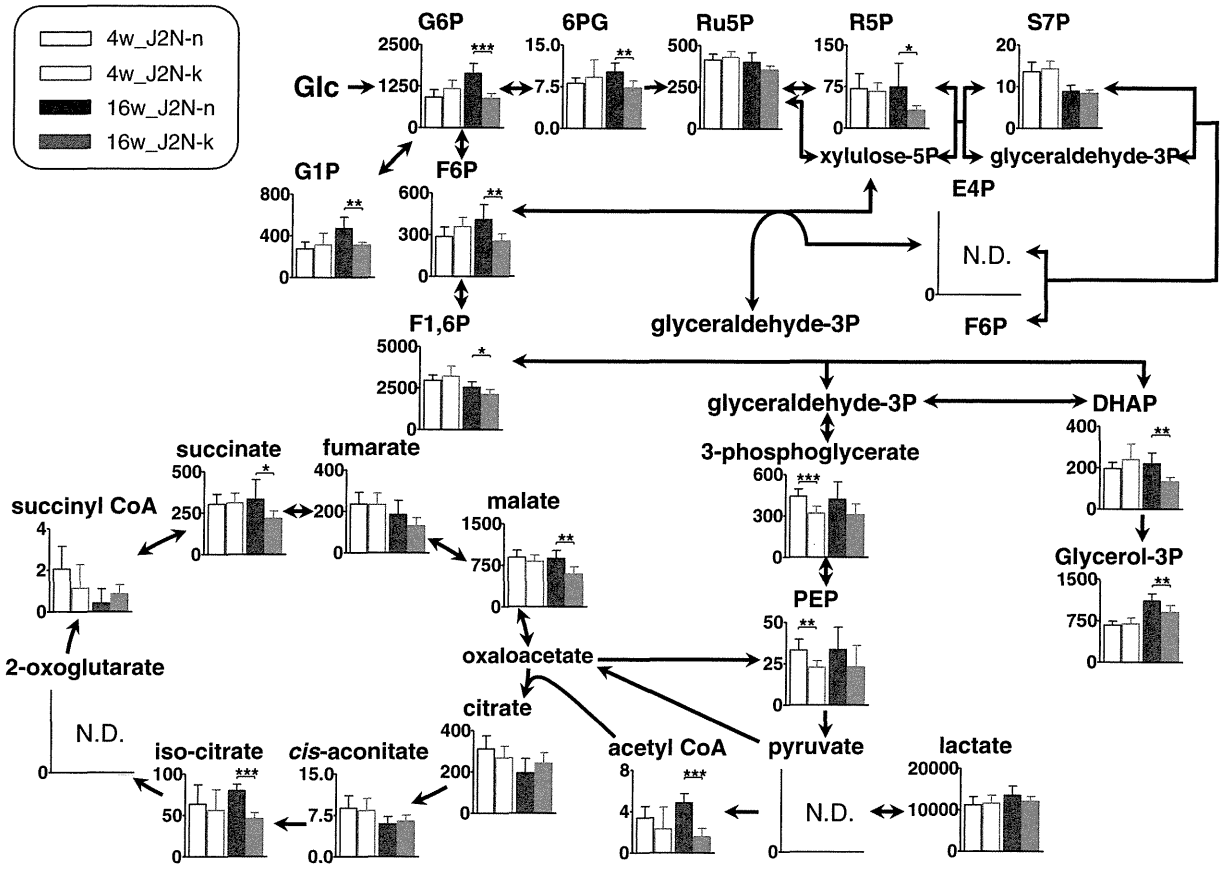

Fig. 2. Metabolome pathway map of quantified charged metabolites, including components of the glycolytic pathway, pentose phosphate pathway, and TCA cycle in J2N-n and J2N-k hamsters at 4 and 16 weeks (4w and 16w). The columns represent average concentrations (nmol/g tissue), and the error bars indicate SD. $^{*}p<0.05$; $^{**}p<0.01$; $^{***}p<0.001$; and N.D., not detected.

significant increase in ornithine levels (1.4-fold, $p=2.3\times10^{-4}$) and a decrease in citrulline levels (0.7-fold, $p=1.1\times10^{-3}$) were also observed in J2N-k hamsters.

3.6. Profiling of lipid metabolites measured by LC-TOFMS

LC-TOFMS detected 1173 peaks and 277 peaks in the positive and negative ion modes, respectively. Relative quantification of the identified metabolites is shown in Supplementary Table 3.

Next, the data were processed for PCA. In the positive ion mode, the 1173 peaks (including unidentified metabolites) were divided into 2 groups on the basis of their retention time (RT): 0.1–37.5 min RT (671 peaks; containing lysophospholipids [lysoPLs], diacylglycerols [DAGs], PLs, SMs, and ceramides [Cers]) and 37.5–60 min RT (502 peaks; containing triacylglycerols [TAGs] and cholesterol esters [ChEs]; Supplementary Fig. 5). PCA was performed separately for each group since PLs and TAGs are the 2 major classes of lipid metabolites in this mode (Supplementary Fig. 6). Distinct clustering of metabolites among the 4 groups (i.e., 4- or 16-week-old J2N-n and J2N-k hamsters) was observed in the data obtained using both positive (0.1–37.5 min RT; Supplementary Fig. 6A) and negative ion modes (data not shown). In contrast, for the second group of metabolites identified in the positive ion mode (37.5–60 min RT), poor discrimination was obtained between all tissue samples (from 4- and 16-week-old J2N-k and J2N-n hamsters) (Supplementary Fig. 6B). These results suggest that the lipid metabolites that were eluted from 0.1 to 37.5 min include candidates for identifying DCM and healthy tissues, even in the presymptomatic phase (4 weeks). Using a p-value threshold of 0.01 for the heatmap, the levels of 34 and 68 metabolites were found to differ between J2N-n and J2N-k hamsters at 4 and 16 weeks, respectively, with 15 overlapping metabolites (Fig. 5).

3.7. Myocardial lipid levels are significantly different in J2N-k and J2N-n tissues

PLs are important components of heart membranes. When focusing on phosphatidylcholine (PC), the levels of many species, most of which contained unsaturated fatty acids, increased in J2N-k compared with J2N-n at the presymptomatic phase (4 weeks). Some of these PC species remained upregulated in the symptomatic phase (16 weeks) (Fig. 5, Supplementary Table 3), including 18:0/20:4PC (1.4-fold, $p=5.4\times10^{-4}$; 1.6-fold, $p=2.0\times10^{-5}$; at 4 and 16 weeks, respectively) and 18:0/22:6PC (1.7-fold, $p=7.0\times10^{-5}$ and 1.7-fold, $p=2.0\times10^{-5}$; at 4 and 16 weeks, respectively). In contrast, levels of several PC species containing linoleic acid (18:2), such as 18:2/18:2PC (0.8-fold, $p=9.4\times10^{-3}$), were reduced at 16 weeks. As for lyso species, a significant increase in the level of 18:0 lyso PC (LPC; 1.4-fold, $p=9.5\times10^{-4}$) was observed in J2N-k at 16 weeks but not at 4 weeks.

Regarding phosphatidylethanolamine (PE) and plasmalogen PE (pPE), the levels of several species containing 22:5 and 22:6 (docosahexaenoic acid, DHA), such as 18:0/22:6PE (1.3-fold, $p=6.1\times10^{-3}$), increased in J2N-k compared with J2N-n hamsters at 4 weeks, although their increase was almost diminished at 16 weeks. At 16 weeks, many species (11 PEs and 8 pPEs) were decreased in J2N-k tissues (Fig. 5, Supplementary Table 3), although 3 PE and 2 pPE species were increased in J2N-k tissues. Notably, species containing linoleic acid (18:2) or eicosapentaenoic acid (EPA; 20:5),

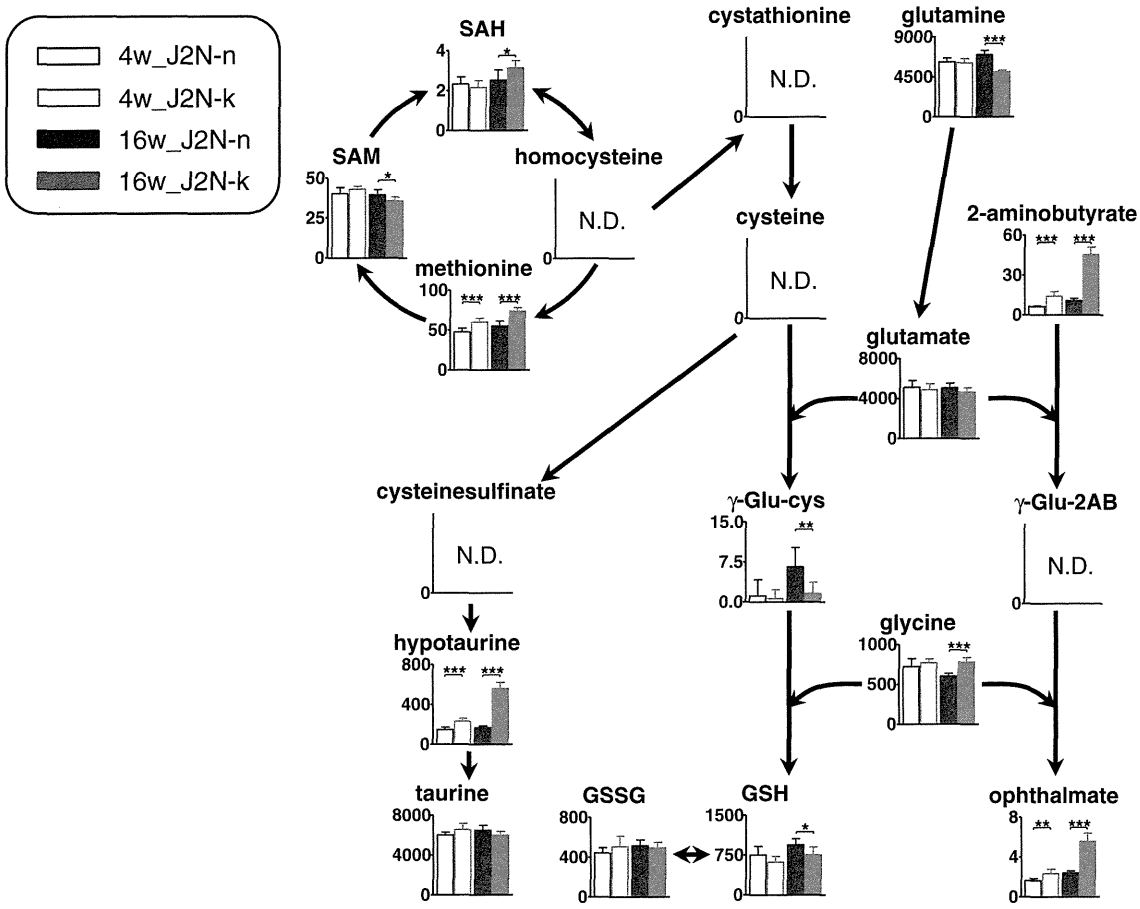

Fig. 3. Quantification of metabolites involved in GSH biosynthesis and related pathways. The columns represent average concentrations (nmol/g tissue), and the error bars indicate SD. $^{*}p<0.05$; $^{**}p<0.01$; $^{***}p<0.001$; and N.D., not detected.

such as 18:1/18:2PE (0.7-fold, $p=1.5\times10^{-3}$), and 18:0p/20:5PE (0.4-fold, $p=1.0\times10^{-5}$), were markedly reduced in J2N-k tissues at 16 weeks. Thus, the levels of PC and PE species commonly containing linoleic acid (18:2) or EPA (20:5) were reduced at the onset of DCM.

Marked differences between the SM levels and their Cer metabolites were observed in the 2 hamster strains at 16 weeks. For example, the levels of 34:1SM (d18:1/16:0; 1.4-fold, $p=5.1\times10^{-4}$) and 34:1Cer (1.4-fold, $p=4.9\times10^{-2}$) increased, but those of 38:1SM (d18:1/20:0; 0.7-fold, $p=3.3\times10^{-3}$) and 38:1Cer (0.6-fold, $p=3.1\times10^{-3}$) decreased in J2N-k tissue as compared to J2N-n tissue.

The levels of major TAG species significantly decreased in J2N-k compared with J2N-n tissues at 16 weeks (Fig. 5, Supplementary Table 3). Although we could not determine the individual fatty acid chain compositions, many of these species were dramatically decreased, including 54:5TAG (0.5-fold, $p=6.0\times10^{-3}$) and 54:6TAG (0.5-fold, $p=5.4\times10^{-3}$). Furthermore, the levels of 9 DAG species

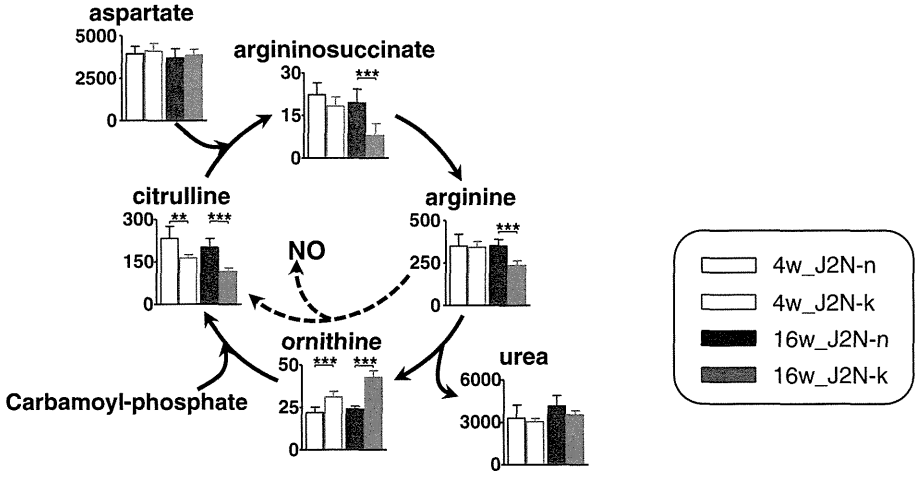

Fig. 4. Metabolic changes in urea cycle metabolism. The dashed lines indicate the NO synthesis pathway, columns represent average concentrations (nmol/g tissue), and error bars indicate SD. $^{*}p<0.05$; $^{**}p<0.01$; and $^{***}p<0.001$.

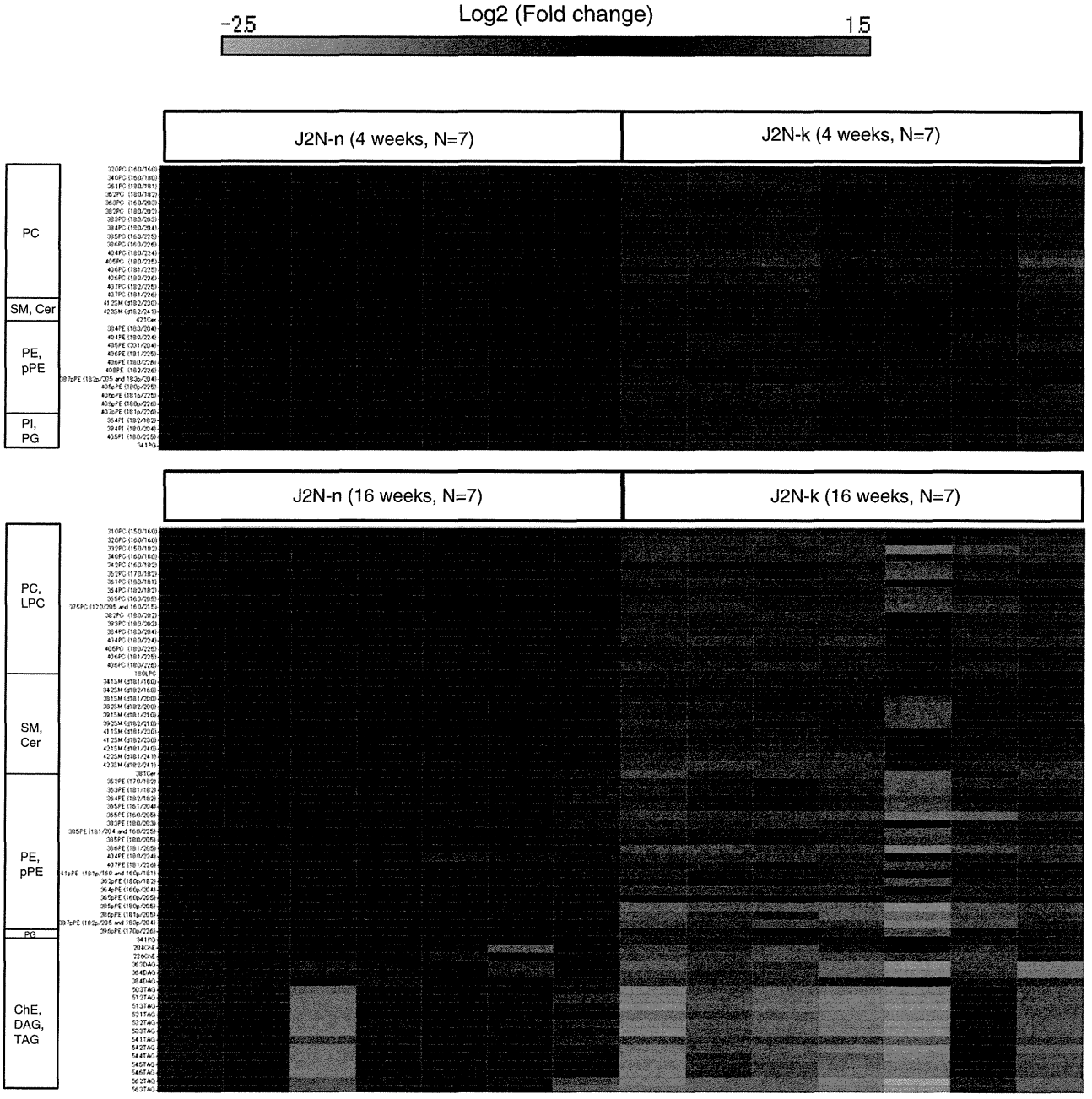

Fig. 5. Heatmap showing relative quantification of lipid metabolites identified in myocardial tissue from J2N-n and J2N-k hamsters ($n=7$ in all groups). Thirty-four (at 4 weeks) and sixty-eight (at 16 weeks) lipid metabolites with different levels ($p<0.01$) in J2N-n and age-matched J2N-k at each time point are shown. Data are represented by the log2 ratio of relative amounts of each metabolite in J2N-k to the mean relative amounts in J2N-n at either 4 or 16 weeks.

changed in J2N-k tissues at 16 weeks: 2 species, including 38:4DAG (1.6-fold, $p=2.4\times10^{-3}$), were increased, while another 7 species, predicted to contain mono- or di-unsaturated fatty acids such as 36:3DAG (0.4-fold, $p=2.2\times10^{-3}$), were significantly decreased.

3.8. Oxidative fatty acids levels were altered in J2N-k myocardial tissues

The levels of 3 prostaglandin (PGs)—PGE_2 (5.1-fold, $p=1.5\times10^{-2}$), PGD_2 (7.8-fold, $p=1.5\times10^{-2}$), and 6-keto-$PGF_{1\alpha}$ (stable metabolite of PGI_2; 8.1-fold, $p=4.6\times10^{-3}$)—were significantly increased in J2N-k myocardial tissue at 16 weeks, compared with J2N-n tissue (Fig. 6, Supplementary Table 4). Moreover, the levels of 12S-hydroxy-5Z; 8E; and 10E-heptadecatrienoic acid (12-HHT), a product of arachidonic acid via the cyclooxygenase pathway, were also increased (5.7-fold, $p=4.7\times10^{-2}$) in these tissues. In addition, levels of cyclooxygenase 2, an enzyme that catalyzes the rate-limiting step of these 4 metabolites, increased at 16 weeks in J2N-k tissue (Supplementary Fig. 7).

3.9. Increased oxidative stress in the DCM heart

Since previous reports, as well as our results (increase in ophthalmate levels), suggest the high oxidative stress levels at 16 weeks of J2N-k hamsters, we assessed lipid peroxidation and superoxide production by 4-HNE staining and DHE staining, respectively (Supplementary Figs. 8 and 9). Results from both staining confirmed an increased oxidative stress in the cardiac tissue of 16-week-old J2N-k hamsters.

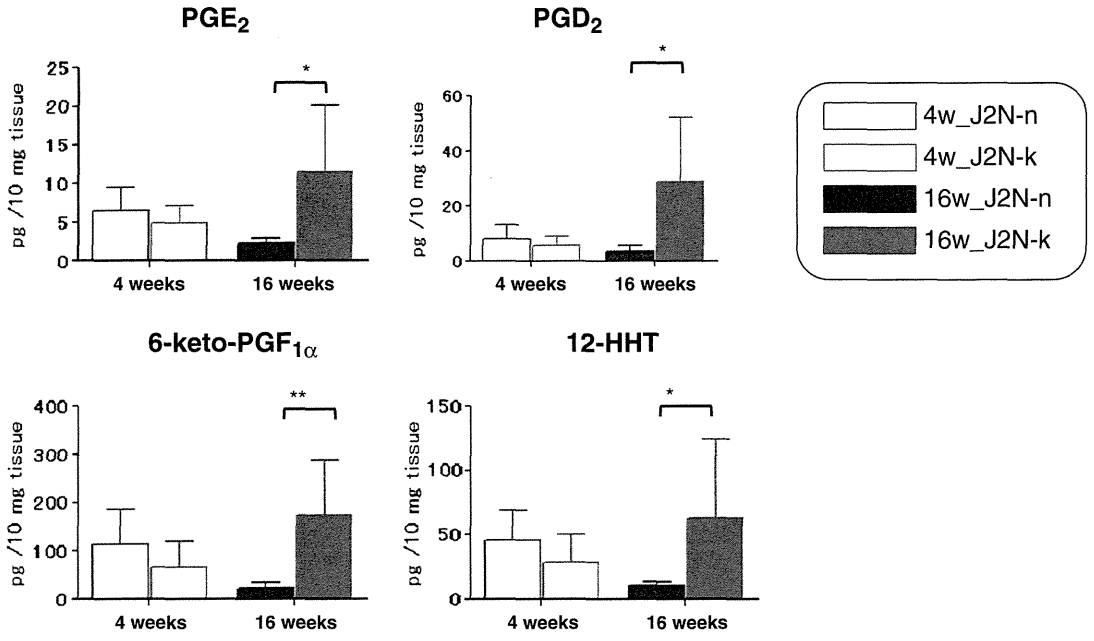

Fig. 6. Levels of 4 eicosanoids in the left ventricular tissues of 4- and 16-week-old J2N-k and J2N-n hamsters. The error bars represent mean ± SD values ($n = 7$). $^{*}p<0.05$, $^{**}p<0.01$, and $^{*}p<0.001$.

4. Discussion

We performed global metabolomic analysis on myocardial tissues from J2N-k cardiomyopathic hamsters, which were found to have significantly different profiles of charged and lipid metabolites from those of J2N-n normal controls. In general, mild edema could be seen in the heart with DCM, and cardiomyocyte protein concentrations in 16-week-old J2N-k hamsters (but not 4-week-old hamsters) decreased by 9.5% compared with the J2N-n line at the same age (data not shown). However, this difference did not have a large impact on the variation in metabolite levels between J2N-k and J2N-n hamsters, and the metabolomic results were shown per tissue weights.

Analysis of charged metabolites showed significant reductions in the levels of glycolysis and TCA cycle metabolites in J2N-k myocardial tissues as compared with those of J2N-n at 16 weeks (symptomatic phase; Fig. 2). In addition to these pathways, the creatine kinase pathway also supplies energy to the heart and maintains ATP levels by the rapid transfer of high-energy phosphoryl groups from phosphocreatine to ADP. Creatine and creatinine (degradation products of phosphocreatine) levels in J2N-k symptomatic phase tissues were significantly lower than those in age-matched controls (Supplementary Table 2). It has been reported that creatine levels are attenuated in heart tissue from dystrophin-deficient *mdx* mice [19] and that creatine levels reflect the severity of heart failure in patients with DCM [20]. In addition, carnitine levels are also significantly decreased in J2N-k tissues at 16 weeks (Supplementary Table 2). Since carnitines are used for transporting fatty acids from the cytosol into the mitochondria, the availability of fatty acids for β-oxidation may be reduced in J2N-k hamsters. This supports our finding that acetyl CoA levels are considerably decreased in J2N-k tissue (ratio of 0.3 at 16 weeks, Supplementary Table 2). A recent paper also reported that Bio-TO2 cardiomyopathic hamster hearts showed reduced activity of pyruvate dehydrogenase [21], which catalyzes acetyl CoA production. These findings suggest that decreased energy production occurs in DCM hearts, resulting in reduced cardiac pumping. Further studies, such as flux analysis, are needed to validate these assumptions.

A mild reduction in GSH levels and a considerable loss of its precursor, γ-Glu-Cys in the glutathione biosynthesis pathway, were observed in J2N-k tissues at 16 weeks. In contrast, mild increases at 4 weeks and considerable increases at 16 weeks were observed for levels of ophthalmate and its precursor, 2-AB in J2N-k tissue (Fig. 3). Ophthalmate is synthesized by the same enzymes as those for GSH, but it contains 2-AB instead of cysteine [10]. Although the cysteine levels in myocardial tissue extracts were below the detection limit, the GSH synthesis pathway appeared to be upregulated based on the increased levels of its components methionine and SAH. Instead of cysteine, our data suggests that the upregulated GSH synthesis pathway uses 2-AB for ophthalmate production. This is supported by changes in the levels of other GSH and ophthalmate synthesis components: glycine levels significantly increased and glutamine (a glutamate precursor) levels decreased. We also observed increased levels of hypotaurine at both 4 and 16 weeks (Fig. 3). Unlike taurine, hypotaurine has antioxidant activity that effectively scavenges hydroxyl radicals and hypochlorous acid moieties [22]. These findings suggest that metabolic changes are initiated to counteract the increased oxidative stress observed in DCM heart tissues as confirmed in Supplementary Figs. 8 and 9.

Significant decreases in the urea cycle metabolites, arginine, argininosuccinate, and citrulline, were observed in myocardial tissues of 16-week-old J2N-k hamsters as compared to J2N-n hamsters (Fig. 4). Reductions in arginine and citrulline levels suggest a reduction in nitric oxide (NO) production by nitric oxide synthase. This is consistent with the report that NO concentrations in coronary circulation were lower in DCM patients as compared to control human subjects [23]. In contrast, increased conversion of arginine to ornithine suggests that the high arginase activity in 16-week-old J2N-k hamsters can modulate NO synthesis by limiting arginine availability for NO synthesis. NO is critical for coupling cardiac excitation-contraction by modulating Ca^{2+} homeostasis [24], suggesting its possible relation to DCM.

A recent study found that changes in lipid homeostasis contribute to the development of various cardiomyopathies [25]. In particular, dysregulation of membrane phospholipid homeostasis alters the interaction of membrane-associated protein complexes that modulate cell signaling and myocardial metabolism [26]. At the presymptomatic phase (4 weeks), we observed increased levels of PC containing unsaturated

(especially polyunsaturated) fatty acids and PE/pPE with 22:5 or 22:6 in J2N-k myocardial tissues (Fig. 5; Supplementary Table 3). In the symptomatic phase, significant decreases in PC containing linoleic acid (18:2) and many PE and pPE species, especially those containing 18:2 and/or EPA (20: 5), were observed in J2N-k hamsters. A significant accumulation of ethanolamine phosphate (1.5-fold, $p = 8.7 \times 10^{-6}$) in J2N-k tissues (Supplemental Table 2 and Fig. 1) suggests that function of the PE biosynthetic enzyme, ethanolaminephosphotransferase, may be impaired in the symptomatic phase tissues. Altered levels of the PC and PE species suggest that membrane perturbations, such as fluidity, are probably important for DCM pathology. Consistent with our results, linoleic acid (18:2) content in PC was reported to be significantly decreased in the myocardium of cardiomyopathic BIO 14.6 hamsters during the development of congestive heart failure [27]. Increased PC content (observed at 4 weeks in this study) was reported to inhibit Ca^{2+}-ATPase (SERCA) activity [28], which was indeed decreased in J2N-k cardiomyopathic hamsters [29]. Our data also show that some LPC species were significantly increased at the DCM symptomatic phase. LPCs increase the intracellular calcium concentration $[Ca^{2+}]_i$ by modulating the activities of the cardiac sarcolemmal membrane ion transporters such as SERCA [30], which may compensate for decreased contractile function. These findings suggest that contractile dysfunction in J2N-k myocardial tissue is partly attributable to aberrant PL metabolism.

At 16 weeks, J2N-k myocardial tissues exhibited altered levels of SMs and Cers of various acyl chain lengths (C16–C24; Fig. 5, Supplementary Table 3), suggesting that specific Cer signaling pathways are activated in DCM. For example, levels of Cer containing palmitic acid (16:0), such as 34:1Cer, were augmented in J2N-k tissue at 16 weeks. As 34:1Cer is a major Cer species and is known to be elevated during apoptosis induced by various agents [31]; it is possible that the apoptosis pathway is triggered in the symptomatic phase. The activation of the apoptotic pathway was reported in proteomic analysis of a phospholamban-mutated DCM mouse model [32].

The PCA of TAGs and ChEs revealed only a modest discrimination between J2N-k and J2N-n tissues both at 4 and 16 weeks (Supplementary Fig. 6B), suggesting wide within-group variations. Nevertheless, remarkable reductions were observed in several major TAG species in J2N-k tissues at 16 weeks (Fig. 5, Supplementary Table 3). TAG is stored in cytosolic lipid droplets within cardiomyocytes and ensures a continuous fatty acid supply for mitochondrial oxidation [33]. Therefore, TAG reductions suggest that heart tissue cannot secure enough energy from fatty acid oxidation, thereby leading to impaired function. Consistent with our observations, fatty acid utilization and oxidation were found to be lower in patients with idiopathic DCM than in normal controls [34]. In addition, DAGs (such as 34:2DAG and 36:3DAG) producing TAGs by diacylglycerol acyltransferase were also significantly decreased at 16 weeks (Supplementary Table 3). We observed decreased levels of glycerol-3-phosphate (a precursor of DAG and TAG, Supplementary Table 2) in J2N-k at 16 weeks, which is consistent with our lipid metabolite data.

The eicosanoids, PGE_2, PGD_2, 6-keto-$PGF_{1\alpha}$, and 12-HHT, produced by the COX pathway, were significantly (more than 5-fold) increased in J2N-k tissues at 16 weeks (Fig. 6). Although eicosanoids are generally thought to contribute to inflammatory responses associated with myocardial dysfunction, recent studies have showed that they may also have a cardioprotective role. For example, increased PGE_2 production protects the heart from ischemia-reperfusion injury via PGE_2 receptors 3 (EP3) and 4 (EP4) [35,36]. Furthermore, mice with cardiac-specific EP4 knockout display a DCM-like phenotype [37]. Elevated PGE_2 production may therefore counteract DCM pathophysiology in J2N-k hamsters. In the DCM transgenic mouse model (Tgalphaq*44 mice overexpressing the activated Galphaq protein), elevated levels of PGI_2, the active precursor of 6-keto-$PGF_{1\alpha}$, compensated for reduced NO-dependent coronary vasodilatation due to endothelial dysfunction during late-stage heart failure [38]. PGI_2 also exerted protective effects on cardiomyocytes during cardiac ischemia-reperfusion injury [39]. Elevation of at least some of these 4 eicosanoids may therefore counteract DCM pathophysiology in the J2N-k model.

5. Conclusions

We performed global metabolomic analysis on left ventricular heart tissues from hamsters with hereditary DCM. In the symptomatic phase, the levels of the most significantly altered charged metabolites are mapped to energy metabolism, the glutathione biosynthesis pathway, and the urea cycle. Specifically, a mild reduction in GSH and a compensatory increase in ophthalmate suggested that increased oxidative stress played a role in DCM pathogenesis; this was later confirmed by 4-HNE and DHE histochemistry. Regarding lipid metabolites, disturbances in membrane phospholipid homeostasis (changes in PC and PE species levels) began even at the presymptomatic phase. The potential involvement of specific eicosanoids in the cardioprotective pathways was suggested by increased levels of these metabolites during the symptomatic phase. Further investigation is required to determine how changes in the concentration of the metabolites identified in this study contribute to cardiac dysfunction in DCM. However, our work does provide insight into the mechanisms involved in DCM pathogenesis and may lead to the identification of new targets for therapeutic intervention or diagnosis.

Abbreviations

2-AB	2-aminobutyrate
4-HNE	4-hydroxynonenal
CE	capillary electrophoresis
Cer	ceramide
ChE	cholesterol ester
DAG	diacylglycerols
DCM	dilated cardiomyopathy
DGC	dystrophin-glycoprotein complex
DHA	docosahexaenoic acid
DHE	dihydroethidium,
EPA	eicosapentaenoic acid
GSH	glutathione
HHT	heptadecatrienoic acid
IS	internal standard
LC	liquid chromatography
LPC	lysoPC
MS	mass spectrometry
NO	nitric oxide
PC	phosphatidylcholine
PCA	principal component analysis
PE	phosphatidylethanolamine
PG	prostaglandin;
PL	phospholipid
pPE	plasmalogen PE
RT	retention time
SM	sphingomyelin
TAG	triacylglycerol
TCA	tricarboxylic acid
TOF	time-of-flight

Supplementary data to this article can be found online at http://dx.doi.org/10.1016/j.yjmcc.2013.02.008.

Funding

This work was supported by the Advanced Research for Products Mining Programme [grant number 10-45] from the National Institute of Biomedical Innovation of Japan to NM, TS, and YS.

Disclosures

None.

References

[1] Luk A, Ahn E, Soor GS, Butany J. Dilated cardiomyopathy: a review. J Clin Pathol 2009;62:219–25.
[2] Tigen K, Cevik C. Beta-blockers in the treatment of dilated cardiomyopathy: which is the best? Curr Pharm Des 2010;16:2866–71.
[3] Takeda N. Cardiomyopathy: molecular and immunological aspects (review). Int J Mol Med 2003;11:13–6.
[4] Seidman JG, Seidman C. The genetic basis for cardiomyopathy: from mutation identification to mechanistic paradigms. Cell 2001;104:557–67.
[5] Campbell KP. Three muscular dystrophies: loss of cytoskeleton-extracellular matrix linkage. Cell 1995;80:675–9.
[6] Yucel D, Aydogdu S, Senes M, Topkaya BC, Nebioglu S. Evidence of increased oxidative stress by simple measurements in patients with dilated cardiomyopathy. Scand J Clin Lab Invest 2002;62:463–8.
[7] Demirbag R, Yilmaz R, Erel O, Gultekin U, Asci D, Elbasan Z. The relationship between potency of oxidative stress and severity of dilated cardiomyopathy. Can J Cardiol 2005;21:851–5.
[8] Baumer AT, Flesch M, Wang X, Shen Q, Feuerstein GZ, Bohm M. Antioxidative enzymes in human hearts with idiopathic dilated cardiomyopathy. J Mol Cell Cardiol 2000;32:121–30.
[9] Mitsuhashi S, Saito N, Watano K, Igarashi K, Tagami S, Shima H, et al. Defect of delta-sarcoglycan gene is responsible for development of dilated cardiomyopathy of a novel hamster strain, J2N-k: calcineurin/PP2B activity in the heart of J2N-k hamster. J Biochem 2003;134:269–76.
[10] Soga T, Baran R, Suematsu M, Ueno Y, Ikeda S, Sakurakawa T, et al. Differential metabolomics reveals ophthalmic acid as an oxidative stress biomarker indicating hepatic glutathione consumption. J Biol Chem 2006;281:16768–76.
[11] Nakamura K, Kusano K, Nakamura Y, Kakishita M, Ohta K, Nagase S, et al. Carvedilol decreases elevated oxidative stress in human failing myocardium. Circulation 2002;105:2867–71.
[12] Fujii T, Onohara N, Maruyama Y, Tanabe S, Kobayashi H, Fukutomi M, et al. Galpha12/13-mediated production of reactive oxygen species is critical for angiotensin receptor-induced NFAT activation in cardiac fibroblasts. J Biol Chem 2005;280:23041–7.
[13] Soga T, Igarashi K, Ito C, Mizobuchi K, Zimmermann HP, Tomita M. Metabolomic profiling of anionic metabolites by capillary electrophoresis mass spectrometry. Anal Chem 2009;81:6165–74.
[14] Soga T, Heiger DN. Amino acid analysis by capillary electrophoresis electrospray ionization mass spectrometry. Anal Chem 2000;72:1236–41.
[15] Bligh EG, Dyer WJ. A rapid method of total lipid extraction and purification. Can J Biochem Physiol 1959;37:911–7.
[16] Taguchi R, Ishikawa M. Precise and global identification of phospholipid molecular species by an Orbitrap mass spectrometer and automated search engine Lipid Search. J Chromatogr A 2010;1217:4229–39.
[17] Sugimoto M, Wong DT, Hirayama A, Soga T, Tomita M. Capillary electrophoresis mass spectrometry-based saliva metabolomics identified oral, breast and pancreatic cancer-specific profiles. Metabolomics 2010;6:78–95.
[18] Ono M, Shitashige M, Honda K, Isobe T, Kuwabara H, Matsuzuki H, et al. Label-free quantitative proteomics using large peptide data sets generated by nanoflow liquid chromatography and mass spectrometry. Mol Cell Proteomics 2006;5:1338–47.
[19] Gulston MK, Rubtsov DV, Atherton HJ, Clarke K, Davies KE, Lilley KS, et al. A combined metabolomic and proteomic investigation of the effects of a failure to express dystrophin in the mouse heart. J Proteome Res 2008;7:2069–77.
[20] Nakae I, Mitsunami K, Yoshino T, Yoshino T, Omura T, Tsutamoto T, et al. Clinical features of myocardial triglyceride in different types of cardiomyopathy assessed by proton magnetic resonance spectroscopy: comparison with myocardial creatine. J Card Fail 2010;16:812–22.
[21] Missihoun C, Zisa D, Shabbir A, Lin H, Lee T. Myocardial oxidative stress, osteogenic phenotype, and energy metabolism are differentially involved in the initiation and early progression of delta-sarcoglycan-null cardiomyopathy. Mol Cell Biochem 2009;321:45–52.
[22] Aruoma OI, Halliwell B, Hoey BM, Butler J. The antioxidant action of taurine, hypotaurine and their metabolic precursors. Biochem J 1988;256:251–5.
[23] Takarada S, Imanishi T, Goto M, Mochizuki S, Ikejima H, Tsujioka H, et al. First evaluation of real-time nitric oxide changes in the coronary circulation in patients with non-ischaemic dilated cardiomyopathy using a catheter-type sensor. Eur Heart J 2010;31:2862–70.
[24] Zima AV, Blatter LA. Redox regulation of cardiac calcium channels and transporters. Cardiovasc Res 2006;71:310–21.
[25] Wende AR, Abel ED. Lipotoxicity in the heart. Biochim Biophys Acta 1801;2010:311–9.
[26] Jenkins CM, Cedars A, Gross RW. Eicosanoid signalling pathways in the heart. Cardiovasc Res 2009;82:240–9.
[27] Okumura K, Yamada Y, Kondo J, Hashimoto H, Ito T, Kitoh J. Decreased 1,2-diacylglycerol levels in myopathic hamster hearts during the development of heart failure. J Mol Cell Cardiol 1991;23:409–16.
[28] Fu S, Yang L, Li P, Hofmann O, Dicker L, Hide W, et al. Aberrant lipid metabolism disrupts calcium homeostasis causing liver endoplasmic reticulum stress in obesity. Nature 2011;473:528–31.
[29] Babick AP, Cantor EJ, Babick JT, Takeda N, Dhalla NS, Netticadan T. Cardiac contractile dysfunction in J2N-k cardiomyopathic hamsters is associated with impaired SR function and regulation. Am J Physiol Cell Physiol 2004;287:C1202–8.
[30] Yu L, Netticadan T, Xu YJ, Panagia V, Dhalla NS. Mechanisms of lysophosphatidylcholine-induced increase in intracellular calcium in rat cardiomyocytes. J Pharmacol Exp Ther 1998;286:1–8.
[31] Pewzner-Jung Y, Ben-Dor S, Futerman AH. When do Lasses (longevity assurance genes) become CerS (ceramide synthases)?: insights into the regulation of ceramide synthesis. J Biol Chem 2006;281:25001–5.
[32] Gramolini AO, Kislinger T, Alikhani-Koopaei R, Fong V, Thompson NJ, Isserlin R, et al. Comparative proteomics profiling of a phospholamban mutant mouse model of dilated cardiomyopathy reveals progressive intracellular stress responses. Mol Cell Proteomics 2008;7:519–33.
[33] Banke NH, Wende AR, Leone TC, O'Donnell JM, Abel ED, Kelly DP, et al. Preferential oxidation of triacylglyceride-derived fatty acids in heart is augmented by the nuclear receptor PPARalpha. Circ Res 2010;107:233–41.
[34] Dávila-Román VG, Vedala G, Herrero P, de las Fuentes L, Rogers JG, Kelly DP, et al. Altered myocardial fatty acid and glucose metabolism in idiopathic dilated cardiomyopathy. J Am Coll Cardiol 2002;40:271–7.
[35] Martin M, Meyer-Kirchrath J, Kaber G, Jacoby C, Flögel U, Schrader J, et al. Cardiospecific overexpression of the prostaglandin EP3 receptor attenuates ischemia-induced myocardial injury. Circulation 2005;112:400–6.
[36] Xiao CY, Yuhki K, Hara A, Fujino T, Kuriyama S, Yamada T, et al. Prostaglandin E2 protects the heart from ischemia-reperfusion injury via its receptor subtype EP4. Circulation 2004;109:2462–8.
[37] Harding P, Yang XP, Yang J, Shesely E, He Q, LaPointe MC. Gene expression profiling of dilated cardiomyopathy in older male EP4 knockout mice. Am J Physiol Heart Circ Physiol 2010;298:H623–32.
[38] Drelicharz L, Kozlovski V, Skorka T, Heinze-Paluchowska S, Jasinski A, Gebska A, et al. NO and PGI(2) in coronary endothelial dysfunction in transgenic mice with dilated cardiomyopathy. Basic Res Cardiol 2008;103:417–30.
[39] Xiao CY, Hara A, Yuhki K, Fujino T, Ma H, Okada Y, et al. Roles of prostaglandin I(2) and thromboxane A(2) in cardiac ischemia-reperfusion injury: a study using mice lacking their respective receptors. Circulation 2001;104:2210–25.

DECREASED SURFACE SIALIC ACID CONTENT IS A SENSITIVE INDICATOR OF MUSCLE DAMAGE

YUKO IWATA, PhD,[1] OSAMU SUZUKI, PhD,[2] and SHIGEO WAKABAYASHI, PhD[1]

[1] Department of Molecular Physiology, National Cerebral and Cardiovascular Center Research Institute, Fujishiro-dai 5-7, Suita, Osaka 565-8565, Japan

[2] Laboratory of Animal Models for Human Diseases, National Institute of Biomedical Innovation, Ibaraki, Osaka, Japan

Accepted 12 August 2012

ABSTRACT: *Introduction*: The glycosylation state of the muscle sarcolemma is crucial for membrane strength and is thereby linked to pathologic conditions. No markers currently exist with sufficient sensitivity to detect muscle damage in biopsy samples. We aimed to determine whether surface sialic acid content is a useful criterion for estimating muscle injury. *Methods*: Sialic acid content was measured by comparing the fluorescence intensity of muscle sections stained with 2 types of lectins. One binds specifically to nonsialylated sugars, and the other binds to both sialylated and nonsialylated sugars. *Results*: Sialic acid levels were markedly reduced (60–80%) in muscles from dystrophin-defective mice, δ-sarcoglycan–deficient hamsters, merosin-deficient mice, and patients with muscular dystrophy, when compared with their healthy counterparts. *Conclusions*: Testing for a marked decrease in sialic acid levels, which is caused by the release of trace amounts of sialidase from damaged muscles, is a sensitive detection method for muscle injury and could be commonly utilized for various subtypes of muscular dystrophy.

Muscle Nerve **47:** 372–378, 2013

Muscular dystrophy is a severe degenerative disorder of skeletal muscle, characterized by progressive muscle weakness.[1] One subgroup of this disease is caused by a defect in the genes that encode for the components of the dystrophin–glycoprotein complex (DGC). This multi-subunit complex spans the sarcolemma to structurally link extracellular matrix proteins, such as laminin, to the actin cytoskeleton, thereby providing mechanical strength to muscle cell membranes.[2,3] Therefore, defects of the DGC result in marked disruption of membrane integrity and/or stability. Sarcolemmal damage accelerates the release of cytoplasmic enzymes or the entry of extracellular substances across the cell membranes. To date, increased serum creatine kinase (CK)[4] levels have been used as an indicator of the extent of muscle damage in patients with Duchenne muscular dystrophy or in corresponding animal models such as dystrophin-deficient mice (*mdx*). However, measurement of serum CK levels is not always a reliable indicator of muscle damage, because they rise and fall rapidly and are easily affected by stresses to the body from surgical procedures, vigorous exercise, or deep intramuscular injections.[5–7] In addition, other cytosolic enzymes released in serum, such as myoglobin, aldolase, or lactate dehydrogenase, have similar limitations with regard to the detection of muscle damage. Furthermore, merosin-deficient mice (*dy/dy*), another dystrophic model representative of human merosin-deficient congenital muscular dystrophy, demonstrated no detectable increase in serum CK levels despite their severe clinical phenotype.[8] Enhanced uptake of externally added Evans blue dye (EBD)[8] as a marker of membrane integrity cannot be used in humans owing to its toxicity; even in animals only postmortem muscle imaging is possible using EBD.

Establishing a diagnosis of muscle damage using biopsy samples and routine analysis is time consuming, even in distinguishing between myopathy and neuropathy. Therefore, newer and simpler methods would be useful for easy detection of muscle damage in various types of muscle degenerative disorders, and the validation of a new diagnostic marker would be invaluable.

Glycosylation has been demonstrated to be intimately linked to muscular dystrophy. Indeed, glycosylation of α-dystroglycan (α-dystroglycan DG), an essential component of the DGC, is critical for its interaction with the extracellular matrix to preserve the mechanical strength of the sarcolemma. Moreover, α-DG interacts with extracellular matrix proteins such as laminin through *O*-mannosyl–linked sialylated tetrasaccharides.[9–11] Abnormal glycosylation of α-DG has been detected in multiple forms of muscular dystrophy in mice and humans.[12,13] Therefore, we hypothesized that a test for changes in glycosylation of the sarcolemma could be used for diagnostic purposes for various types of muscular dystrophy.

Sialic acid (a generic term for neuraminic acid derivatives) is an important carbohydrate expressed on the terminal ends of glycan structures in many cell surface glycoproteins and glycolipids, where they mediate various cellular functions (e.g., cell–cell or cell–matrix interactions)[14] and are essential for mammalian survival, development, and growth.[15,16] Sialic acids are ultimately

Abbreviations: ACL, *Amaranthus caudatus* lectin; α-DG, α-dystroglycan; CK, creatine phosphokinase; DAPI, 4′,6-diamidino-2-phenylindole dihydrochloride; DGC, dystrophin–glycoprotein complex; *dy/dy*, merosin-deficient mice; EBD, Evans blue dye; FITC, fluorescein isothiocyanate; Galβ1,3GalNAc, galactose-(β1,3)-*N*-acetylgalactosamine; J2N-k, δ-sarcoglycan–deficient hamsters; J2N-n, control hamsters; *mdx*, dystrophin-deficient mice; PNA, peanut agglutinin; RT, room temperature; WT, wild-type

Key words: lectin staining, muscle injury, muscular dystrophy, sialic acid, sialidase

Correspondence to: Y. Iwata; e-mail: yukoiwat@ri.ncvc.go.jp

Published online 16 August 2012 in Wiley Online Library (wileyonlinelibrary.com). DOI 10.1002/mus.23632

transferred to oligosaccharide chains by the catalytic function of a large family of sialyltransferase enzymes. Conversely, the removal of sialic acid moieties is catalyzed by sialidase. The cytosolic fraction of skeletal muscles exhibits a higher level of sialidase activity than do other tissues.[17] Therefore, if sialidase is released from damaged muscle, it would greatly affect biological processes by changing the conformation of glycoproteins and uncovering or masking the binding sites of functional glycomolecules. Conversely, in distal myopathy with rimmed vacuoles (hereditary inclusion body myopathy), mutation of genes involved in the biosynthesis of sialic acids has been reported.[18–20] These findings raise the possibility that reduction in sialic acid levels has important pathological significance and may also be exploited as a sensitive detection method to monitor release of sialidase in various types of muscle degenerative disorders.

In this study, we addressed whether surface sialic acid content could be altered in muscular dystrophy.

METHODS

Materials. Biotinylated peanut agglutinin (PNA) lectin, *Amaranthus caudatus* lectin (ACL), and fluorescein isothiocyanate (FITC-avidin D; Vector Laboratories, Burlingame, California) were used according to manufacturer's instructions. The sialidase used was isolated from *Clostridium perfringens* (Sigma Chemical Co., St. Louis, Missouri). Alexa Fluor 647 goat anti-mouse IgG (H+L; Invitrogen, Carlsbad, California) and FITC-PNA (Vector Laboratories) were also used in several experiments.

Animals. Delta (δ)-sarcoglycan–deficient hamsters (J2N-k), a model of human δ-sarcoglycanopathy, and age-matched control hamsters (J2N-n) were purchased from Japan SLC, Inc. (Shizuoka, Japan). Four-week-old *dy/dy* and *mdx* mice and age-matched controls (wild-type [WT]) were purchased from the Jackson Laboratories (Bar Harbor, Maine). All animal experiments were performed in accordance with the animal experimentation guidelines of the National Cerebral and Cardiovascular Center (NCVC), Japan.

Human Tissues. Tissue samples were obtained from skeletal muscle biopsy specimens from the NCVC from patients with muscular dystrophy and by autopsies of patients without muscle failure as controls.[21] Written informed consent was obtained from all subjects.

Staining of Skeletal Muscle Sections with Lectins. The sugar chain properties in frozen sections (approximately 5–6 μm) of skeletal muscles were analyzed by the binding of biotinylated PNA or ACL, as described previously.[22] Frozen sections were fixed in 100% ethanol for 10 min at room temperature (RT). After washing with phosphate-buffered saline, the sections were incubated with each biotinylated lectin (10 μg/ml) for 15 min at RT. When sialidase treatment was performed, the sections were treated with 0–5000 mU of sialidase in 50 mM sodium acetate (pH 5) for 2 hours at 37°C before incubation with lectins. These lectins were visualized by incubating the sections with 20 μg/ml of FITC-avidin D for 5 min at RT, followed by observation under a fluorescence microscope (IX81; Olympus, Tokyo, Japan) equipped with confocal capability (Fluoview FV1000; Olympus). For greater time savings, the fixed sections were stained directly with FITC-PNA (10 μg/ml) for 15 min at RT. The nucleus was stained with 4′,6-diamidino-2-phenylindole dihydrochloride (DAPI; Dojindo Laboratories, Kamimashiki-gun, Japan).

Quantification of Fluorescent Intensity Visualized with Lectin Staining. Images of serial sections stained with lectins were analyzed by investigators blinded to the genotypes, using NIH Image software. The entire region covering each fiber and the region covering only the intracellular space in cross-sections were selected visually, and their fluorescence intensities were measured. Fluorescence intensity corresponding to the sarcolemmal region was calculated by subtracting the intensity of the intracellular region from that of the total area. All data were expressed as mean ± standard deviation (SD) unless otherwise indicated. Differences between the groups were determined using the Student *t*-test. $P < 0.05$ was considered statistically significant.

RESULTS

To specifically detect the sialylated sugar group, 2 types of lectins, PNA and ACL, were used. The PNA lectin specifically binds to nonsialylated galactose-(β1,3)-*N*-acetylgalactosamine (Galβ1,3GalNAc) moieties on oligosaccharide groups on glycoproteins or glycolipids, but not to sialylated sugar moieties (Fig. 1A). By contrast, ACL interacts with sialylated and nonsialylated forms of Galβ1,3GalNAc structures (Fig. 1A). Therefore, the amount of sialylated sugars can be measured easily by comparative staining between PNA and ACL in the plasma membrane (Fig. 1A). This strategy was applied to skeletal muscles from J2N-k and J2N-n hamsters. Skeletal muscles from both types of hamster were well stained with ACL (Fig. 1B and C), indicating that both types of sarcolemma express similar apparent levels of Galβ1,3GalNAc. By contrast, the